Spring 2019

Three-Dimensional Collagen Tubes for In Vitro Modeling

Rebecca Jones

THREE-DIMENSIONAL COLLAGEN TUBES FOR IN VITRO MODELING

by

Rebecca Jones

Bachelor of Science
University of South Carolina, 2013

Submitted in Partial Fulfillment of the Requirements

For the Degree of Doctor of Philosophy in

Biomedical Engineering

College of Engineering and Computing

University of South Carolina

2019

Accepted by:

Richard L. Goodwin, Major Professor

John F. Eberth, Committee Member

Daping Fan, Committee Member

Robert L. Price, Committee Member

Cheryl L. Addy, Vice Provost and Dean of the Graduate School

ACKNOWLEDGEMENTS

I would like to acknowledge Lorain Junor for all of her help from when I was just starting out as an undergraduate student to the end of my graduate research with her limitless knowledge and help in imaging among many other areas.

I would also like to acknowledge Katrina Harmon for her unending support, encouragement, and guidance no matter what the hour was with so many experiments that yielded both successes and failures.

I would also like to acknowledge my mom and the rest of my family for instilling my core values and work ethic in me as well as supporting me throughout these years and celebrating my accomplishments no matter how big or small.

ABSTRACT

Collagen type I represents a novel material for three-dimensional in vitro models. While two-dimensional models are typically inadequate for recreating the complex processes of the body, collagen provides a three-dimensional basis with a variety of applications, including remodeling of vascular cells under tension and vascular stenosis. Smooth muscle cells reorganize and reconstruct their environment differently under conditions of tensions, such as with sutures, or under conditions without applied external tension. Vascular stenosis, the abnormal narrowing of blood vessels, arises from defective developmental processes or atherosclerosis-related adult pathologies. Stenosis triggers a series of adaptive cellular responses that induces adverse remodeling, which can progress to partial or complete vessel occlusion with numerous fatal outcomes. Despite its severity, the cellular interactions and biophysical cues that regulate this pathological progression are poorly understood. Here, we report the design and fabrication of a three-dimensional (3D) in vitro system to model cellular tension from sutures and vascular stenosis so that specific cellular interactions and responses to hemodynamic stimuli can be investigated. Tubular cellularized constructs (cytotubes) were produced, using a collagen casting system, to generate a straight cylindrical model in addition to stenotic arterial model. Spatial distribution of cells remained more even in cylindrical cytotubes that were sutured compared to those without applied tension. Fabrication methods were developed to create cytotubes

containing single- and co-cultured vascular cells, where cell viability, distribution, morphology, and contraction were examined. Fibroblasts, bone marrow primary cells, smooth muscle cells (SMCs), and endothelial cells (ECs) remained viable during culture and developed location- and time-dependent morphologies. We found stenotic cytotube contraction to depend on cellular composition, where SMC-EC co-cultures adopted intermediate contractile phenotypes between SMC- and EC-only cytotubes. Our fabrication approach and the resulting in vitro and artery models can serve as 3D culture systems to investigate vascular pathogenesis and promote the tissue engineering field.

TABLE OF CONTENTS

LIST OF FIGURES

CHAPTER 1

INTRODUCTION[1]

Vascular stenosis is a common condition broadly characterized as abnormal blood vessel narrowing, which results in increased resistance to blood flow. During development, this process can have major implications for overall cardiovascular health in conditions such as supravalvular aortic stenosis.[1,2] While vascular stenosis can occur in arteries and veins, it occurs mostly in medium- and large-sized arteries.[3] Vascular stenosis also refers to the geometry of an artery and is not a disease in and of itself but can be triggered or caused by an underlying disease or defects in the tissue. It can also arise as a result of interventions such as transannular patch repair, which is known to cause left pulmonary artery stenosis in patients with tetralogy of Fallot.[4] Alternatively, atherosclerotic conditions such as carotid artery disease, peripheral artery disease, or renal artery disease are characterized by plaque accumulation resulting in significant luminal narrowing.[5–7] Atherosclerosis is a precursor and major risk factor for the majority of acute coronary syndromes (ACS), which are triggered by sudden drops in blood flow to the heart and often lead to death or severe complications. These events

[1] Parts of this chapter have been excerpted from the following research article:

1. Jones RS, Chang PH, Perahia T, et al. Design and Fabrication of a Three-Dimensional in Vitro System for Modeling Vascular Stenosis. *Microsc Microanal*. 2017;23(4):859-871. doi:10.1017/S1431927617012302

are also classified under the category of general cardiovascular disease (CVD), which accounted for 788,000 deaths in 2010 or 32 percent of overall deaths in the United States for that year. Coronary heart disease, a subcategory of CVD that is more specifically linked to atherosclerosis, was the predominant form of CVD in 2010, resulting in 380,000 of the 788,000 CVD deaths. In total, atherosclerosis-related diseases were responsible for 68% of CVD deaths in 2010.[8] According to the American Heart Association, CVD accounted for 30.8 percent of overall deaths in the United States in 2013, or approximately one death every 40 seconds, with 46.2% attributed to coronary heart disease resulting in about one out of every seven deaths.

In order to reduce the prevalence and mortality of atherosclerosis and its related diseases, the sequence of events leading to the development and escalation of atherosclerosis must be better defined so that researchers can derive efficient preventive measures and treatments for clinicians. Many years of research have contributed to the current depth of knowledge for this disease, yet the precise process and pathways in which atherosclerosis appears and progresses remain ambiguous and vague.

In recent years, the biomechanical forces from blood flow within arteries have gained more recognition as key determining factors in the location and the likelihood of occurrence for atherogenesis.[9,10] Further investigation into these biomechanical forces in relation to atherosclerosis may help define the mechanisms through which the disease initiates and progresses. Biomechanical stimuli were previously thought to play very minor roles in biological phenomena

and to have few effects on chemical signaling and other phenomena.[11,12] Recent research in this area and other areas of biology has proven that biomechanical stimuli and cellular mechanotransduction play a much larger role in mechanical and chemical cellular signaling and behavior than scientists had previously believed.[12]

As blood flows through arteries, the viscous property of blood exerts a force upon the layer of endothelial cells that comprise the innermost layer of the vessel wall called the tunica intima. This tangential frictional force, measured in Pascals (Pa) or Newtons per meter squared (N/m^2), on the intimal layer is referred to as wall shear stress (WSS) or endothelial shear stress (ESS) and occurs as a result of blood flowing across the endothelial cell layer.[10,12] Wall shear stress (τ_w) is represented as the product of the blood viscosity and the velocity gradient at the wall in the radial direction ($\tau_w = \mu \frac{dv}{dr}$).[10,13] Pulsatile pressures normal to the blood flow confer cyclic stretching within the vessel wall that is also referred to as cyclic strain, which then induces a circumferential stress upon the vessel wall.[12,14] Smooth muscle cells (SMCs) and elastic and collagen fibers located in the medial layer of the vessel wall supply the mechanical strength of the arterial wall, thereby accommodating the circumferential stress and cyclic strain forces, while the outer adventitial vessel layer, composed of mainly fibroblasts and collagenous fibers, contributes to wall reinforcement.[14,15] Animal models of surgically induced aortic stenosis have also been used to investigate the transient, proximal and distal effects of altered hemodynamics.[16,17] The increased resistance to flow raises blood pressure, causing cardiac hypertrophy, while local downstream flow disturbances

also exacerbate stenosis progression provoking further stenosis and vascular damage.[7,18,19] Despite the wide variety in etiology, a common series of sequelae occurs in vascular pathology, which is characterized by remodeling of the extracellular matrix and excessive smooth muscle proliferation.[5,19] Without intervention, this pathology will progress, leading to critical stenosis, occlusion, and, potentially, vessel rupture.[6,7] Though the general outcomes of this progression are well characterized, numerous aspects of the mechanistic cell–cell interactions that drive vascular pathology and its progression are unknown.

While in vivo investigations appear to be ideal, multi- organ system responses and subject-to-subject anatomical and physiological variation complicate analysis and interpretation. Alternatively, in vitro experiments using standard two-dimensional cell culture fail to adequately model the complex, in vivo, tissue behaviors of blood vessels.[20] Endothelial cell (EC) activation, smooth muscle cell (SMC) proliferation, and extracellular matrix (ECM) remodeling appear to be part of a concerted pathological process that involves each of the representative vascular cells, including ECs, SMCs, and fibroblasts (FBs), through multifactorial and heterotypic cell signaling cascades.[20,21] Thus, the purpose of this study was to generate an in vitro, three-dimensional (3D) arterial model capable of supporting the growth and development of an array of characteristic vascular cells in an environment that can provide dynamic mechanical stimuli.

Nearly 35 years ago, a type I collagen-based blood vessel model was proposed as a novel material for an in vitro blood vessel model.[22] Type I collagen is the most abundant type of collagen in the adult human connective tissues, thus

it seems like a logical choice when attempting to generate 3D models that recreate conditions in the body. Since then, type I collagen has been utilized for countless in vitro tissue models, not limited to applications for the cardiovascular field, connective tissues, mesenchymal stem cells, and many others.[23–25]

In previous studies, we generated a variety of 3D models of cardiovascular tissues using a variety of fabrication techniques.[26–28] More recently, a dynamic fluid flow bioreactor system was used in conjunction with a tubular collagen scaffold to investigate the mechanisms that regulate hemodynamic-driven remodeling in developing valve tissues.[29,30] During development, hemodynamic stimuli regulate remodeling in the cardiovascular valve tissues and also in the early vasculature in the mammalian yolk sac.[31] A similar interaction between cardiovascular and vascular remodeling also exists with disease, in which altered blood flow from heart defects can incite maladaptive remodeling and plaque accumulation in downstream arteries later in life.[19] From our prior work and the work of others, it is apparent that mechanical loading and 3D environment play a pivotal role in the behavior of cells embedded within the vascular walls or on the surface of these matrices, yet the molecular mechanisms, which regulate the mechanotransduction pathways involved in the initiation and the progression of several types of pathology, have yet to be determined[20,29–32] Within the appropriate 3D physical environment, these pathological conditions can be studied in an in vitro setting, thereby elucidating novel mechanistic processes not previously substantiated with conventional culture models.

Here, we report the design and fabrication of cellularized collagen tubular constructs (cytotubes) that support representative vascular cells in an environment capable of fostering dynamic stimuli and cellular adaptation. Experiments were carried out to examine the effect of cellular tension on cells in these 3D collagen gels. Contraction analysis showed these cylindrical cytotubes decreased in both length and diameter when statically cultured without adding suture tension. Spatial distribution of cells within cytotubes under cellular tension also remained more uniform as compared to those under no external tension.

Collagen cytotubes containing different cell types, including FBs, bone marrow primary cells (BMPCs), SMCs, and ECs, were analyzed for cell viability, morphology, distribution, and structural contraction using static and dynamic culturing techniques. Characterization of the cytotube cultures featured robust growth and morphogenesis of vascular cells. The spatial distribution of cells within collagen constructs changed as a function of time, with the exterior surface area becoming increasingly occupied by f-actin. Analysis of cellularized collagen tube contraction showed that constructs containing a combination of SMCs and ECs contracted more than EC-only constructs, but less than SMC-only cytotubes, indicating that heterotypic, cell–cell interactions play an important role during histogenesis. These results support the premise that this collagen fabrication technique is capable of producing cellularized constructs with multiple vascular cell types and specific 3D geometries. The technique can also be used in combination with our novel fluid flow bioreactor culturing system to further investigate the

cellular, molecular, and mechanical mechanisms of vascular development and disease in a dynamic in vitro culturing system.

CHAPTER 2

MATERIALS AND METHODS[2]

2.1 CYLINDRICAL AND VASCULAR STENOSIS CYTOTUBE FABRICATION

2.1.1 Collagen Isolation

As initially described in Yost et al (2004), bovine dermis was cut into 4×6 cm strips and frozen before processing. All superficial epidermis was removed prior to washing the collagen with running water. The collagen was incubated overnight at 4°C in 2% $Ca(OH)_2$ per hide weight then mixed well and placed in a tumbler. After another incubation period in 4°C, the collagen was washed under running water and placed in a 1 M NaCl solution and put back in 4°C conditions. The collagen was adjusted to a pH of 5 with a 1 M HCl solution then washed with deionized water until the conductivity was at 100 μS/cm. The hides were then cut in 1 in^2 pieces and placed in cold 0.5 M acetic acid solution. Pepsin was added at a 50:1 hide weight to pepsin ratio followed by incubation at 4°C overnight. The collagen was ground in a clean meat grinder with ice then mixed with 0.5 M acetic acid solution and pH-adjusted to between 3.0 and 4.5 using 1 M HCl solution. After incubating overnight at 4°C again, the pH was adjusted to 3.0 and added to a clean

[2] Parts of this chapter have been excerpted from the following research article:

1. Jones RS, Chang PH, Perahia T, et al. Design and Fabrication of a Three-Dimensional in Vitro System for Modeling Vascular Stenosis. *Microsc Microanal*. 2017;23(4):859-871. doi:10.1017/S1431927617012302

press. Cold 0.5 M acetic acid was mixed in with the pressed collagen. A solution of 1 M NaCl was added to the liquid until the collagen came out of the solution followed by another overnight incubation at 4°C. The collagen was then spun down at 5000 to 7000 rpm for 30 minutes to remove the water and pH-adjusted to 5.5 with 1 M NaOH. The collagen was put into dialysis tubing and then placed in cold water in 4°C until the conductivity read 50 μS/cm. After processing, the collagen concentration was adjusted to a dry weight/wet weigh concentration of 1.25-2.77% by adding water and pH-adjusted to approximately 4.9 by adding 0.5 M HCl. The collagen was sterilized with 1,200 rad γ-irradiation before being used to fabricate the tube constructs.

2.1.2 Cell Culture and Cellular Suspension

For the cylindrical cytotubes, human primary aortic smooth muscle cells obtained from ATCC (ATCC PCS-100-012) were cultured with the vascular smooth muscle cell growth kit (ATCC PCS-100-042) containing the vascular cell basal medium (ATCC PCS-100-030) with 5 ng/mL rh fibroblast growth factor (FGF)-basic, rh insulin, rh epidermal growth factor (EGF), 50 μg/mL ascorbic acid, 10 mM L-glutamine, 5% fetal bovine serum, 25 ng/mL amphotericin B, 10 units/mL penicillin, 10 μg/mL streptomycin, and 33 μM phenol red. Cells were cultured at 37°C, 5% CO_2 in 100 mm petri dishes. The growth medium was changed every other day to replenish nutrients and remove waste.

A cell line, derived from primary cultures of adult rat heart FBs, was used as a source of cardiovascular FBs for the initial characterization studies of the vascular stenosis cytotubes. Rat BMPCs, derived from isolated bone marrow stem

cells, were used to promote vasculogenesis within the cellularized collagen constructs.[33] These cells, along with rat aortic SMCs and ECs, were grown in Dulbecco's modified Eagle medium (DMEM) containing 10% fetal bovine serum, 1% penicillin/streptomycin, and 0.1% amphotericin B at 37°C, 5% CO2 in 100 mm petri dishes. The growth medium was also changed every other day to replenish nutrients and remove waste.

To prepare the cellular suspension for seeding, confluent plates of cells were trypsinized (0.05% trypsin/0.02% ethylenediaminetetraacetic acid (EDTA) for human SMCs and 0.25% trypsin/0.1% ethylenediaminetetraacetic acid (EDTA) for rat cell types), pelleted via centrifugation, and re-suspended in fresh growth medium. The concentrations of the cellular suspensions were calculated using a hemocytometer (Bright-Line™, Sigma-Aldrich®, Horsham, PA, USA). Cytotubes were made using approximately one half of a confluent 100 mm plate of cells to account for variation in size among different cell types. Cylindrical cytotubes were made using 3.0×10^6 SMCs per tube. For the vascular stenosis cytotubes using rat cell types, average cell concentrations for cytotubes were 3.01×10^6 for FBs, 3.32×10^5 for SMCs, 4.1×10^6 for ECs, and 4.3×10^6 for BMPCs.

2.1.3 Cellularized Collagen Polymerization Technique

Since polymerization of collagen occurs in the pH range of 6.0–8.0, and the optimum pH for cells is typically 7.4, polymerization of the collagen and the subsequent shift in pH had to be achieved in a manner that did not compromise cell viability.[34,35] HEPES (4-(2-hydroxyethyl)piperazine-1-ethanesulfonic acid) buffer (10 mM HEPES, 0.14 M NaCl, 4.7 mM KCl, 1.3 mM $MgSO_4$, 1.6 mM $CaCl_2$),

a widely used supplement in DMEM or other growth medium to maintain physiological pH values, was chosen as the reagent to polymerize the solubilized collagen gel while raising the final pH to 7.4. To find the most suitable alkalinity of the neutralizing reagent, a range of 10× HEPES buffers, with different pH values from 7.4 to 8.1 in 0.1 increments, were added to solubilized collagen at an 8:1:1 volumetric ratio (1.2 mL solubilized collagen: 150 µL 10× HEPES: 150 µL cell suspension for cylindrical cytotubes and 1.0 mL solubilized collagen: 125 µL 10× HEPES: 125 µL cell suspension for vascular stenosis cytotubes). The pH values of the collagen mixtures were measured again after mixing thoroughly to determine which HEPES buffer solution produced the final desired collagen pH of 7.4.

Prior to polymerization, the collagen was slightly acidic with pH values ranging from ~5.12 to 6.64 due to variation between batches of collagen. To compensate for the fluctuations, a lookup table was created to determine the alkalinity of 10× HEPES buffer necessary to obtain the final pH value of 7.4. Figure 2.1 depicts examples for collagen solutions with pH of 5.27, 5.95, and 6.64, which would require 10× HEPES buffers of pH 7.84, 7.70, and 7.55, respectively, to produce a final pH of 7.4.

From this empirical data, an equation (equation 2.1) was created to determine the appropriate pH of the 10× HEPES buffer to combine with the acidic pH of the collagen in order to achieve the desired final pH of 7.4. In this equation, “x” represents the value of the initial pH of the solubilized collagen, and “y” represents the pH of the 10× HEPES buffer that is needed to have an end pH of

7.4 after mixing the collagen containing the cell suspension and the HEPES buffer together.

$$y = -0.21169x + 8.9569 \qquad \text{Equation 2.1}$$

2.1.4 Casting Molds

For the cylindrical tubes, the lumen of the collagen tube construct was created using stainless steel rods that were engineered as a simple straight, cylinder as seen in Figure 2.2. For the vascular stenosis cytotubes, the lumen of the collagen tube construct was created using stainless steel rods that were micromilled with a pin and socket connection, which, when joined together, formed an axisymmetric constriction in the center of the tubular mold. The pin and socket apparatus allowed for the casting of the stenotic region of the tube lumen, in which the diameter was reduced from 3.0 to 0.65 mm, while also facilitating the removal of the steel rods from the collagen construct without disrupting the integrity of the cellularized material (Figs. 2.3 a, b). The 8:1:1 ratio mixture of the collagen, 10× HEPES buffer, and cell suspension was used as the casting material for the tube. A collagen concentration of at least 1.0% was found to be necessary to maintain construct integrity during the casting process. Collagen tubes with concentrations <1.0% did not retain the shape of the mold, as shown in Figure 2.3c with tubes made from 0.67% collagen. Increasing the collagen concentration improved structural integrity (Figs. 2.3 d, e) until the collagen became too viscous to syringe into the molds.

Dialysis tubing specialized for high permeability (Spectra/Por® 2, MWCO 12–14 kDa, Spectrum) was used as the exterior sheath or outer casing to aid in

osmotic pressure optimization and rapid small molecule exchange, while retaining the collagen molecules within the dialysis tubing. Dialysis tubing of 10mm flat width was cut into pieces measuring 5 cm in length. Prior to tube assembly, the sheaths were sterilized with 1,200 rad γ-irradiation and submerged in 10× HEPES buffer at a pH of 7.4 to soften them.

2.1.5 Collagen Wall Fabrication

The cytotube constructs contained a range of cell type combinations located within the collagen gel wall, in the tube lumen, or in both the wall and the lumen. For the human SMCs, the straight cylindrical collagen tubes contained only SMCs within the collagen wall. For the rat cell types, the following cell type combinations were used in cytotube fabrication: FB-only (wall), FB-BMPC (wall), SMC-only (wall), EC-only (lumen), and SMC-EC (wall and lumen). FB-only, SMC- only, EC-only, and SMC-EC co-cultured cytotubes were used in static dish cultures while the FB-BMPC cytotubes were used in the static and dynamic bioreactor cultures as described in the Static and Dynamic Culturing section. Cellular seeding of the collagen wall and casting of the collagen tube were done simultaneously. The luminal seeding for EC-only and SMC-EC co-cultured cytotubes was performed after fabrication of the collagen wall and is described in more detail in the next section.

To make the cellularized collagen mixture, 1-1.2 mL of the collagen gel was loaded into a 1.5mL microcentrifuge tube using a syringe and then mixed with 125-150 µL filter-sterilized 10× HEPES buffer; 125-150 µL of the desired cell type suspension was then added to the neutralized collagen gel and mixed thoroughly.

Collagen tubes for vascular stenosis that did not contain cells within the wall were formed using only collagen with 125 µL of 1× HEPES buffer at a pH of 7.4, which was added to the collagen mixture in lieu of the cell suspension, in addition to the 125 µL of 10× HEPES buffer in order to maintain a consistent collagen concentration for cytotubes with different cell combinations.

Microcentrifuge tubes containing either type of collagen mixture (cellular or acellular) were centrifuged for ~10 s to remove air bubbles within the gel. The mixture was slowly syringed into the mold with one end capped to avoid bubble formation, which would compromise the integrity and uniformity of the construct. Once filled, a cap was placed at the other end of the tube, before submerging the entire mold in a sterile plastic culture tube (17 × 125 mm, Fisherbrand™, Pittsburgh, PA, USA) containing cell media. Each mold was incubated at 37°C, 5% CO2 in the plastic culture tube in the media for 24 h to allow for collagen polymerization (Fig. 2.4a).

2.1.6 Vascular Stenosis Cytotube Luminal Seeding

Following collagen wall polymerization, the dialysis tubing and internal mold rods were gently removed from the cytotubes. Collagen tubes containing ECs within the lumen were seeded by pipetting 100 µL of cell suspension into the lumen at each end of the construct. Afterwards, the luminally seeded cytotubes were placed in sealed culture tubes containing media and affixed to a tube rotator (099A RD5512; Glas-Col®, Terre Haute, IN, USA) that revolved at 17 rpm at 37°C, 5% CO2 for 24 h (Fig. 2.4b). The cytotubes were positioned horizontally so that the axial direction of the tubes was parallel to the rotational axis of the rotator, which

allowed for even seeding of cells on the lumen of the construct. The co-cultured cytotubes with SMCs within the wall and ECs in the lumen were synthesized by making the cellularized collagen wall first and subsequently seeding the lumen with ECs using the rotator-assisted seeding technique.

2.1.7 Static and Dynamic Culturing

After fabrication of the cytotubes, each construct selected for static dish culture was transferred into a 60 mm petri dish and cultured in growth medium at 37°C, 5% CO2 (Fig. 2.4c). The cytotubes were maintained in static dish culture for periods ranging from 24 h to 7 days with the culture media being changed every 48 h.

A custom-designed fluid flow bioreactor (Adams & Chittenden Scientific Glass®, Berkeley, CA, USA) was used in addition to static culturing in petri dishes. The cylindrical cytotubes containing only human SMCs within the collagen wall were mounted in the bioreactors using sutures to examine the effect of sutures on the cytotubes as compared to the non-sutured cytotubes that were examined in static petri dish culture.

To determine the effects of flow on cells within the wall of the stenotic tubes, cytotubes containing FBs and BMPCs within the tube wall were examined using static and dynamic culture in the fluid flow bioreactor. The FB-BMPC combination was used instead of FB-only cytotubes to evaluate the ability of the BMPCs to promote vasculogenesis under the condition of applied flow as compared with no flow. For both static and dynamic bioreactor culturing, the FB-BMPC cytotubes were sutured onto the bioreactor as depicted in Figure 2.4d.[29,30] Static bioreactor

culturing referred to constructs in bioreactors, which were not attached to any pumps, whereas tubes selected for dynamic culturing were sutured in bioreactors attached to pumps to receive applied flow. Cytotubes in dynamic bioreactor cultures received an average volumetric flow rate of 3.33×10^{-9} m^3/s. The flow rate, which is lower than typical stenotic conditions for arteries of this scale, was chosen to minimize pressure on the cytotube wall so that any changes in cell morphology could be directly attributed to flow rather than flow and pressure collectively. Furthermore, continuous flow was used to provide steady-state flow conditions in order to minimize ambiguities encountered when analyzing the results. Cytotubes of both culture types were removed from the bioreactors after 48 h of culture and processed for microscopy.

2.2 CONTRACTION ANALYSIS AND IMAGING

2.2.1 Contraction Measurement and Statistical Analysis

During the static culturing phases, the cylindrical cytotubes with human SMCs were imaged after 0, 1, 3, and 7 days of static culture. The SMC-only, EC-only, and SMC-EC co-cultured stenotic cytotubes were imaged daily to examine the effects of the characteristic vascular cells on the collagen construct. The dimensional changes in the tube diameter and length over a 7 or 10-day time period were measured using NIH ImageJ software. Data were reported as means with at least three independent experiments per treatment, and error bars represent standard error of the mean. Statistical significance for the human SMC-only cytotubes was determined using a one-way analysis of variance (ANOVA) with repeated measures while the stenotic cytotubes were analyzed via a two-way

ANOVA. Both sets of cytotubes underwent Tukey's multiple comparisons test with α values of 0.05. Differences between the group means were considered significant at $p < 0.05$.

2.2.2 Confocal Microscopy Sample Preparation and Imaging

After culture to specific time points, cytotubes were fixed in 4% paraformaldehyde/phosphate buffered saline (PBS) at 4°C for at least 24 h.

Cylindrical cytotubes were processed and embedded in paraffin before being sectioned at thicknesses of 6-8 μm with a microtome. Slides were de-paraffinized in xylene and rehydrated in decreasing concentrations of ethanol before staining. Cytotubes for vascular stenosis were embedded in 5% agarose/PBS gel and sectioned longitudinally using a vibratome at thicknesses of 150–200 μm. The sections were permeabilized with 0.1-0.25% Triton X-100/PBS for 20min and washed with PBS three times, followed by blocking in 2% bovine serum albumin (BSA)/PBS for 1 h at room temperature.

Immunofluorescent labeling was used to identify cell phenotypes. Regardless of cell type, vascular stenosis cytotube sections were stained with fluorescently labeled phalloidin (F-actin stain, Alexa Fluor 488®, no. A12379; Life Technologies™, Carlsbad, CA, USA), 4′6-diamidino-2-phenylindole (DAPI, nuclear stain, no. D21490; Invitrogen™, Carlsbad, CA, USA), and Cy3-labeled α smooth muscle actin (Cy3-αSMA, no. C6198; Sigma-Aldrich®) overnight at 4°C. Cylindrical cytotube sections were stained with phalloidin and DAPI as well. The sections were washed three times with PBS for 10 min each, then mounted on glass slides with 1,4-diazabicyclo[2.2.2]octane (DABCO, no. D2522; Sigma-

Aldrich®). The cylindrical cytotubes were imaged with confocal imaging (Zeiss LSM 510 Meta; Carl Zeiss, Thornwood, NY, USA) and with the Invitrogen EVOS FL Auto Cell Imaging System (Carlsbad, CA, USA). Vascular stenosis cytotube sections were only imaged with confocal microscopy.

Confocal image stacks for vascular stenosis sections were collected in the X, Y, and Z dimensions from 200 μm thick vibratome sections. Individual image stacks were first collapsed in the Z dimension to a single projection resulting in images that were 450 × 450 μm. These were then tiled using Photoshop (Adobe®, San Jose, CA, USA) into transverse strips across the constriction nozzle regions, enabling the visualization of intact vibratome sections in a single image.

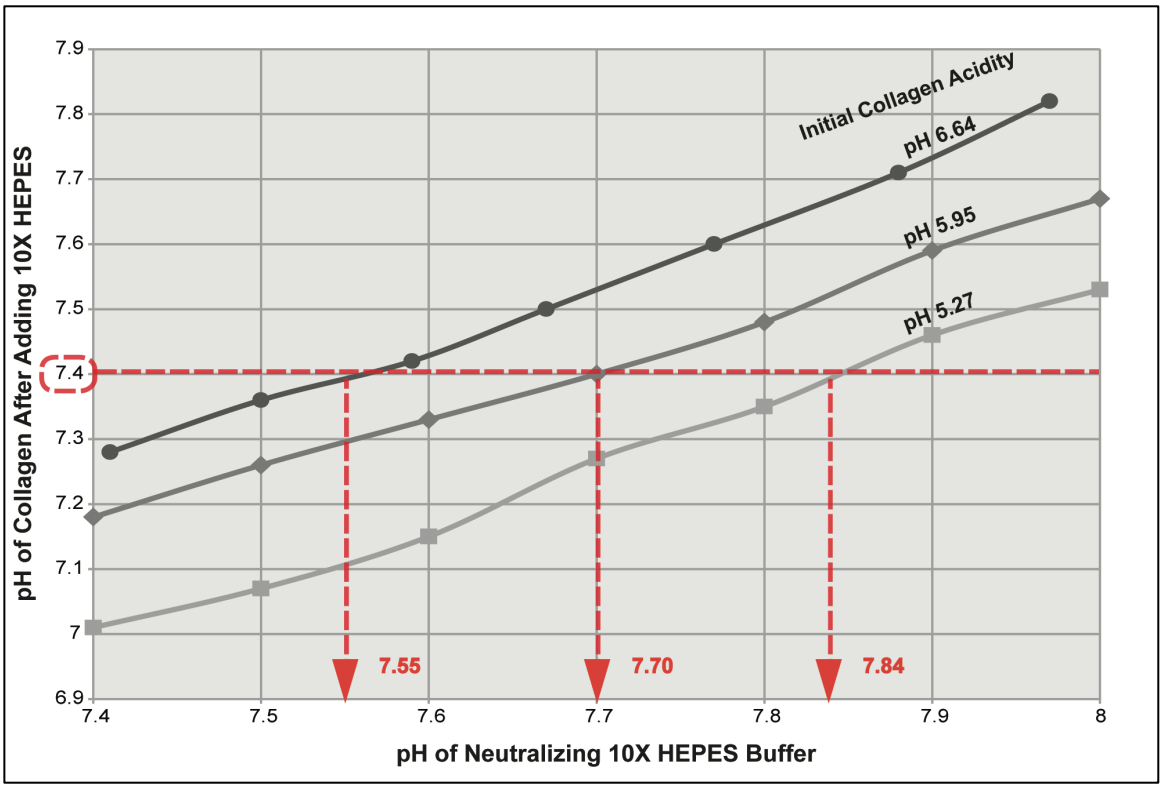

Figure 2.1 A lookup table for collagen polymerization was developed because the desired final pH of 7.4 for the collagen mixture before adding the cell suspension required estimating the appropriate pH value of 10× HEPES buffer in order to neutralize the collagen, which was initially acidic but varied in pH value between batches. The pH of the neutralizing buffer can be found at the intersection of where the line for initial collagen acidity passes through the horizontal dashed line representing a final pH of 7.4. Examples are shown for initial collagen pHs of 5.27, 5.95, and 6.64, which, respectively, require 10× HEPES buffers of pH 7.84, 7.70, and 7.55 to produce a final pH of 7.4 before adding the cell suspension. Values were determined via interpolation of the three standard curves shown.

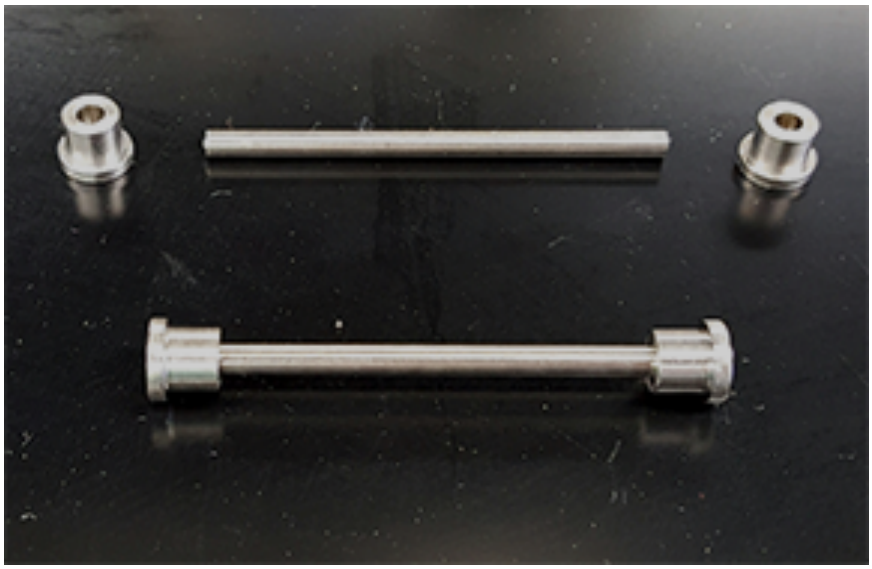

Figure 2.2 The stainless steel mold engineered with interlocking socket ends to mold the lumen of the cylindrical cytotubes. The design allows for the removal of the stainless steel mold while maintaining the collagen construct after it has polymerized.

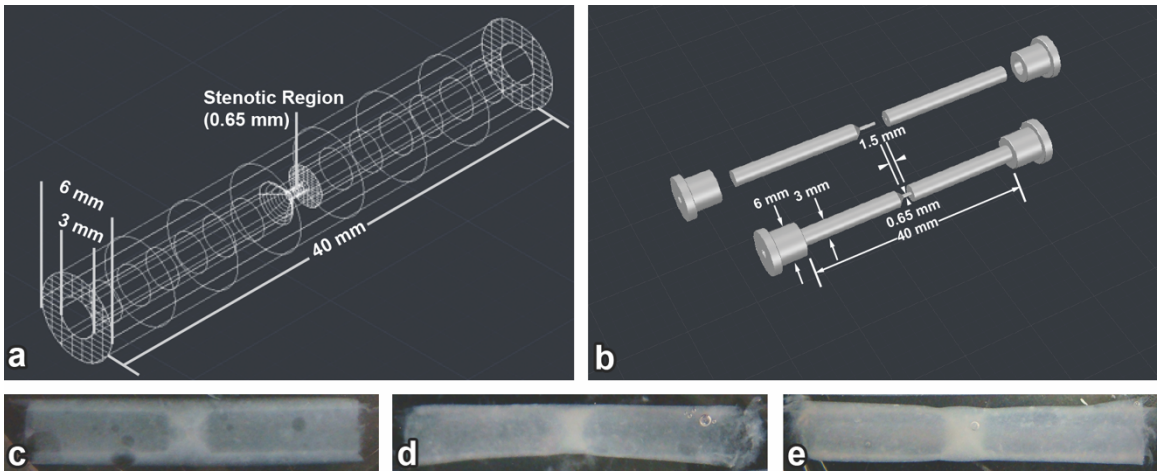

Figure 2.3 A schematic of the collagen construct cast using the stenotic vessel design (a) shows the axisymmetric stenotic region in the tube lumen where the diameter is reduced from 3.0 to 0.65mm. Stainless steel rods with interlocking pins and sockets formed the dimensions of the inner lumen and stenotic region of the collagen tubes (b). Cytotube constructs made with 0.67% (c), 1.0% (d), and 1.8% (e) collagen type I, respectively, show that a collagen concentration of 1.0% or more was necessary for the cytotubes to maintain the shape of the mold.

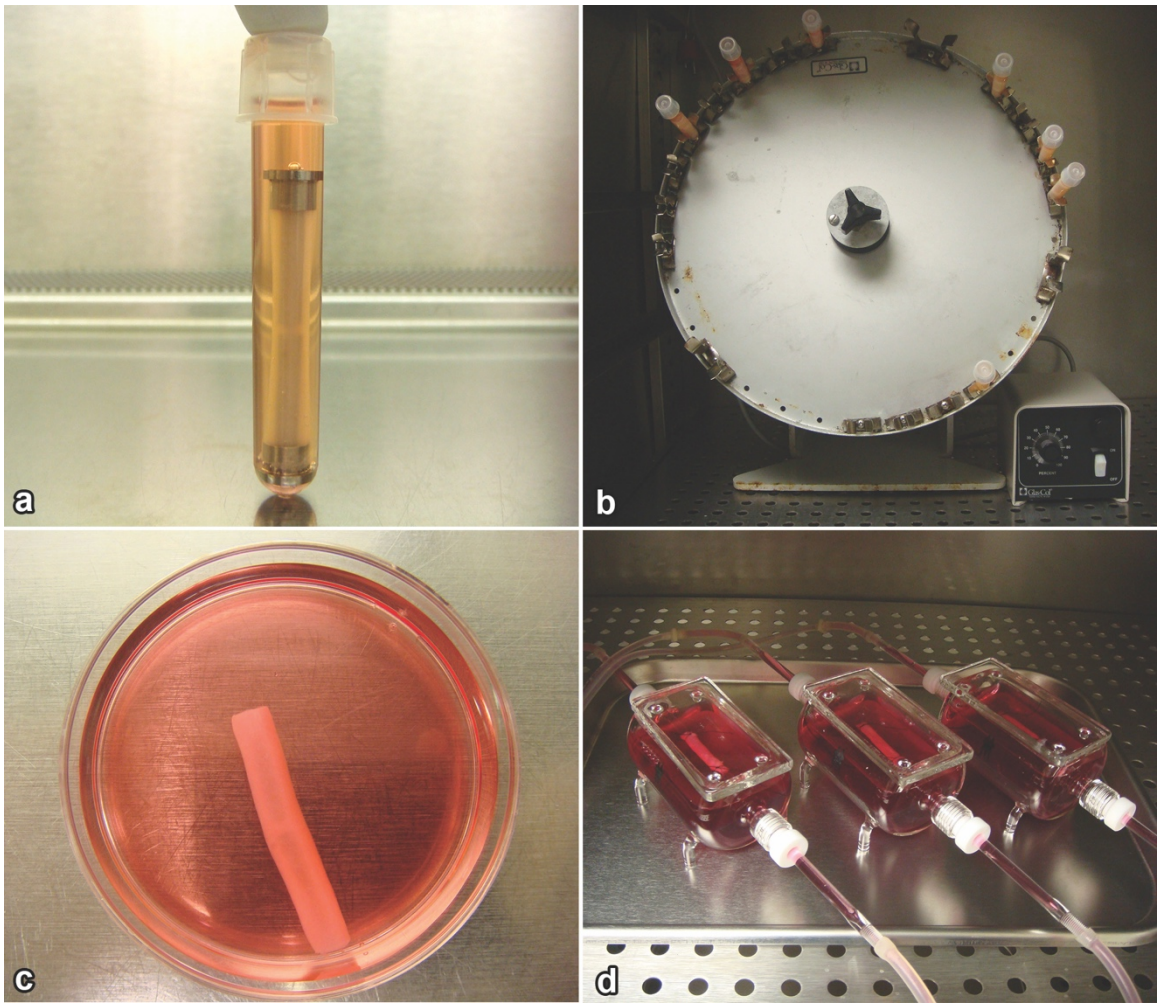

Figure 2.4 Collagen tubes containing cells within the wall and in the lumen were fabricated via a two-step process in which the cells within the wall were produced via casting, and then the lumen was seeded with cells. Cytotube constructs that have been cast around the stainless steel mold and dialysis tubing were placed in culture tubes for 24 h to allow for collagen polymerization (a). Luminally seeded cytotubes were placed on the rotator-assisted luminal cell seeding apparatus inside a tissue culture incubator for 24 h (b). Cytotube constructs could be cultured in petri dishes (c) or mounted within the bioreactors for culturing (d).

CHAPTER 3

RESULTS[3]

3.1 CYLINDRICAL CYTOTUBE RESULTS

3.1.1 Comparison of Sutured and Non-Sutured Cylindrical Cytotubes

Cytotubes containing only human SMCs within the collagen gel wall were cultured in bioreactors with sutures holding the tubes in place and compared to those cultured in petri dishes without sutures (contraction tubes). Immunofluorescence staining with DAPI to visualize the cell nuclei allowed for the depiction of cell distribution within the cytotubes after 1, 3, and 7 days of their respective culture conditions. As illustrated in figure 3.1, there were very few differences between the cytotubes cultured with and without sutures. After three days of culture, the cells that had been sutured were shown to have a more even cellular distribution throughout the length of the collagen tube as compared to the cytotube that had been cultured statically in a petri dish, which showed a lack of cellularization in the middle of the tube (Figure 3.2). This trend continued as depicted in day 7 of culture (Figure 3.3) where cells in the contraction tube

[3] Parts of this chapter have been excerpted from the following research article:

1. Jones RS, Chang PH, Perahia T, et al. Design and Fabrication of a Three-Dimensional in Vitro System for Modeling Vascular Stenosis. *Microsc Microanal*. 2017;23(4):859-871. doi:10.1017/S1431927617012302

appeared to be clustered towards one end of the collagen tube rather than the middle or the other end of the tube as indicated by the blue staining for DAPI.

3.1.2 Contraction of Cylindrical Cytotubes

The cylindrical cytotube constructs containing only SMCs were observed to contract over time in length and diameter while in static dish culture for seven days (Fig. 3.4). The contractile behavior of cells was most pronounced in cytotubes in length rather than diameter. The differences in mean length contraction amounts were significant between Day 1 and Day 3 and Day 1 and Day 7 with no significant differences for between Day 3 and Day 7 for p-values of $p < 0.05$. The tube length at Day 1 was $94.28 \pm 1.05\%$ of the original tube length at Day 0. Interestingly, the greatest amount of contraction in length occurred between Days 0 and 1, with a reduction of 5.75% while Day 1 to Day 3 saw a reduction of 5.26% to yield $88.98 \pm 0.91\%$ of the Day 0 tube length. Day 3 to Day 7 saw the smallest contraction amount to produce a length that was $88.12 \pm 0.82\%$ of the initial tube measurement.

Analysis of tube diameter contraction found that SMC-only cytotubes also showed decreases in the outer diameter of the tube, however these decreases were not as pronounced as the reduction in length. Mean differences of the contraction diameter were significant between Day 1 and Day 3 as well as between Day 1 and Day 7, however there was no significance in the outer diameter reduction between Day 3 and Day 7 for $p < 0.05$. The greatest amount of contraction, similar to the length data, occurred between Day 0 and Day 1 with a 3.79% decline in the original outer diameter values to yield $96.21 \pm 0.84\%$. From

Day 1 to Day 3, the tubes contracted 2.55% to 93.66 ± 0.71% of the initial outer diameter. By Day 7, the tubes remained at 92.64 ±0.94% of the starting diameter.

3.2 VASCULAR STENOSIS RESULTS

3.2.1 Characterization of Stenotic Cellularized Constructs

3.2.1.1 FB-Only Cytotubes

Initially, cytotubes seeded with only FBs within the wall were used to verify the viability of cells within the collagen constructs. Phenotypical changes associated with time in culture for FBs growing within the collagen wall of the scaffold are shown in Figure 3.5. On day 1 (Figs. 3.5a, 3.5b), the cells within the collagen displayed a rounded, retracted shape typical of trypsinized cells. On day 2 of culture (Figs. 3.5c, 3.5d), the FBs within the collagen matrix exhibited a morphology that was more stellate in shape, which is typical of mesenchymal cells. Days 3 and 4 of culture showed cells within the wall with more exaggerated stellate morphologies (Figs. 3.5e, 3.5g), whereas cells near the luminal surface of the constructs aligned along the edges of the wall and showed increased expression of f-actin based on staining intensity (Figs. 3.5f, 3.5h). By day 5, the FBs were more densely associated within the wall (Fig. 3.5i) and at the luminal surface with visible assembled layers of flattened, squamous cells (Fig. 3.5j) with intracellular actin stress fibers (Fig. 3.5j, top arrow) and organized αSMA filaments (Fig. 3.5j, bottom arrow). After 1 week, cells within the collagen matrix of the tube wall were overall more mesenchymal in morphology (Fig. 3.5k), whereas a cross-sectional view of the construct showed an epithelial-like organization of cells on the luminal surface of the cytotube (Fig. 3.5l). The increasing cellular alignment and f-actin

network organization over time can be observed by comparing the fenestrated layer in day 3 with the more confluent layers in days 4 and 6 (Figs. 3.5f, 3.5h, 3.5l).

3.2.1.2 EC-Only Cytotubes

Rat aortic ECs were seeded onto the lumen of cytotubes using the rotational seeding method as described earlier. On day 1, after 24 h of rotational culture, globular clusters of polygonal cells with dense f-actin networks were found on the luminal side of the cytotube (Figs. 3.6a, 3.6b). On day 2, the globular clusters of ECs were elongated along the wall edge (Fig. 3.6c); however, other cell clusters displayed cortical actin filaments aligned with adjacent cells along the luminal boundary, implying the formation of cell–cell junctions, an important characteristic of endothelial barrier function (Fig. 3.6d). Increasingly confluent areas of squamous endothelium were observed on the luminal surface of the cytotubes at day 5 and 7 of static culture (Figs. 3.6e–h). An additional feature of note is the expression of αSMA by some of the ECs in several of the time points shown in Figure 3.6. While αSMA is traditionally considered to be a marker of SMCs, it has also been found in some ECs in the luminal surface of the human, rat, and mouse thoracic aorta and in ECs undergoing endothelial-to-mesenchymal transition (EndMT).[36] EndMT is the process by which ECs acquire mesenchymal markers such as αSMA and neural–cadherin and gain migratory and invasive capacities while losing cell–cell junctions and EC markers such as CD31 and vascular–endothelial–cadherin. EndMT is essential for arterial development and tissue regeneration but also plays a role in tissue fibrosis and other pathological processes including atherosclerosis.[37] Although the exact reason for the αSMA

expression here is unknown, it can be said that the ECs in the cytotube exhibited more than one phenotype.

3.2.1.3 SMC-Only Cytotubes

Collagen cytotubes containing only SMCs within the wall and no cells in the lumen were cast using the techniques mentioned above. Figure 3.7 shows images from vibratome sections of the SMC-only cytotubes that were assembled by tiling transverse sections from the exterior wall up to the constriction nozzle region. Representative cytotube cultures are shown for days 1, 3, 5, and 7. On day 1, SMCs within the collagen were rounded, as was observed for the same time point for the FB cultures in Figure 3.5. Initially, SMCs were dispersed throughout the collagen matrix of the construct. At days 3, 5, and 7, SMCs transitioned in shape and location from uniformly spherical to spindle-like on the luminal side and stellate near the outer wall. In addition, an increasingly confluent layer of aligned SMCs formed along the longitudinal direction of the cytotube while fewer cells remained near the luminal wall (Fig. 3.7).

3.2.2 Contraction of EC, SMC, and SMC-EC Co-Cultured Cytotubes

The cytotube constructs containing characteristic vascular cells were observed to contract over time in length and diameter while in static dish culture. The contraction of SMC-only, EC-only, and SMC-EC co-cultured cytotubes was examined over a 10-day culture period (Fig. 3.8). The contractile behavior of cells was most pronounced in cytotubes seeded with only SMCs (Fig. 3.8a). EC-only cytotubes exhibited the smallest contraction amount in length (8.34 ± 2.1%) as compared with the other two groups, whereas both SMC-only and SMC-EC co-

cultured cytotubes showed much greater reductions in length (Fig. 3.8b). While SMC-only cytotubes became on average 58.95 ± 1.6% shorter in length after 10 days of static culture, the SMC-EC co-cultured cytotubes decreased only 29.95 ± 2.4% in length during that same time period, suggesting that the presence of ECs limited the ability of the SMCs to contract or adapt the construct. The differences in mean length contraction amounts were significant for all culture types at days 6 and 10 with no significant differences for any culture type at day 2 for p-values of $p < 0.05$.

Analysis of tube diameter contraction found that, interestingly, SMC-only and SMC-EC cytotubes showed increases from the original tube outer diameter at day 2, which could have been indicative of a compensatory mechanism for the initial decreases in length or early SMC expansion and adaptation of the tube wall (Fig. 3.8c). Consistent with the pattern of length contraction, the greatest decrease in diameter occurred in SMC-only cytotubes with 56.81 ± 1.5% followed by SMC-EC cytotubes with 24.45 ± 2.5% and EC-only cytotubes with 11.05 ± 4.7%. Mean differences of the contraction diameter were only significant at day 10 for SMC versus SMC-EC and SMC versus EC for $p < 0.05$.

3.2.3 Dynamic Culturing of Cytotubes with FBs and BMPCs

After cytotubes with characteristic vascular cells in static dish culture demonstrated robust growth and morphogenesis for FBs, SMCs, and Ecs, we sought to examine the effect of flow with vasculogenesis via static and dynamic bioreactor cultures, using our previously-described custom fluid flow bioreactor system.[29,30] For initial characterization of the bioreactor-cultured tubes, we chose

to use co-cultures of FBs and BMPCs cast within the wall in order to examine whether the BMPCs would differentiate in cytotubes cultured under flow compared with no- flow cultures. The FB-BMPC cytotubes selected for dynamic culturing were mounted in the bioreactors, which were attached to pumps that applied steady-state flow at an average volumetric flow rate of 3.33×10^{-9} m^3/s for 48h. No-flow controls were mounted onto bioreactors that were not connected to pumps and cultured for 48h. As depicted in Figure 3.9, cells in the cytotubes cultured with flow aligned along the edges of the collagen construct, whereas cytotubes that were not subjected to flow showed cells distributed across the entire width of the wall. In addition, constructs with flow exhibited αSMA that was more aligned and organized along the edge of the collagen wall despite the presence of more pronounced αSMA in control samples (Fig. 3.9). Cytotubes cultured with flow also showed more interconnected networks of cells. In general, only a few differences were observed between the flow and no-flow cytotube constructs cultured in bioreactors and could be due to the low flow rate, the absence of applied pressure, or lack of pulsatile flow. Cells in both the flow and no-flow groups were similar to the static cultured FB constructs in Figure 3.5 in their morphology and in the expression pattern of αSMA.

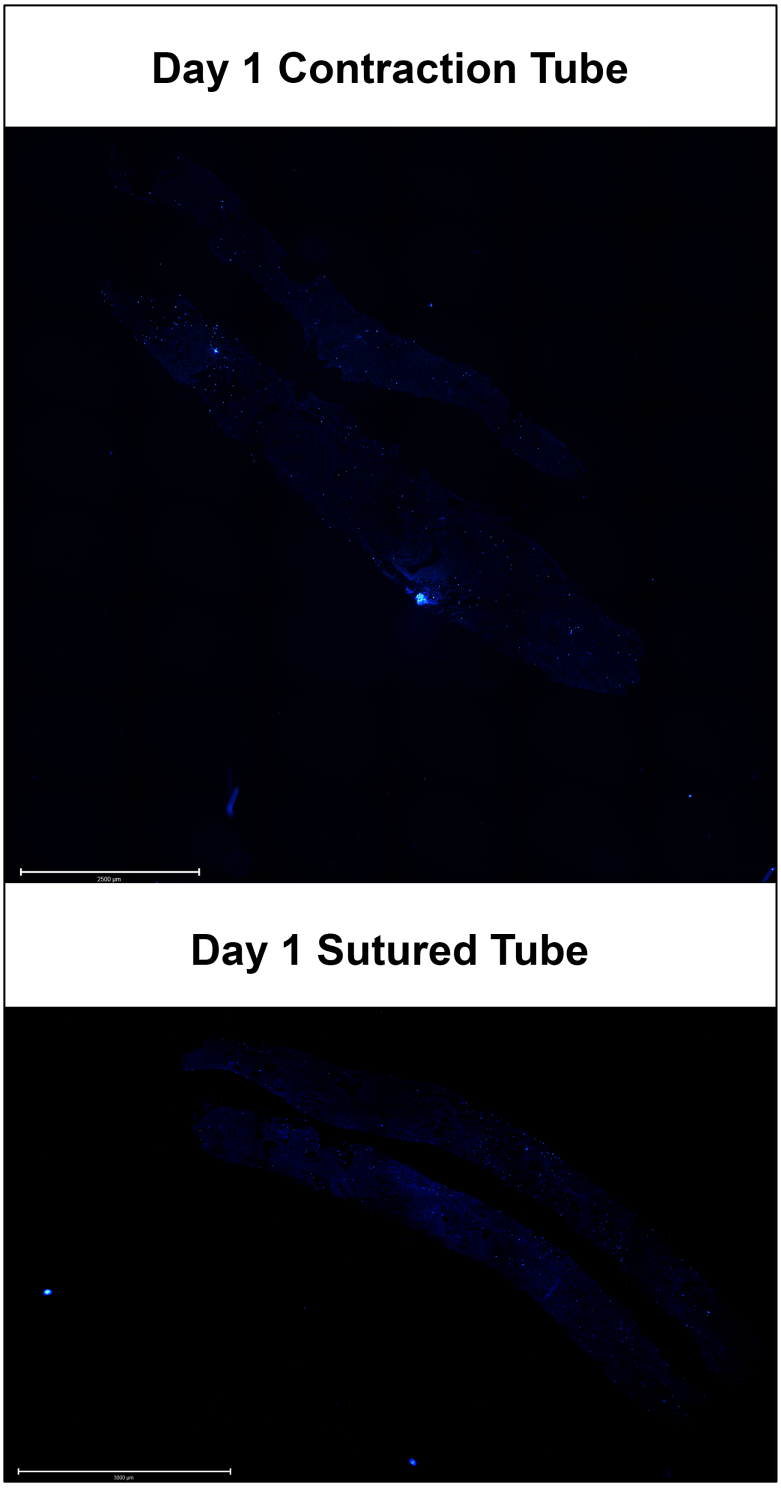

Figure 3.1 SMCs seeded within the collagen wall of cytotubes cultured without sutures in static petri dishes showed very few differences in cellular distribution as depicted by DAPI staining intensity (blue staining, cell nuclei) compared to SMCs in cytotubes that were sutured in bioreactors.

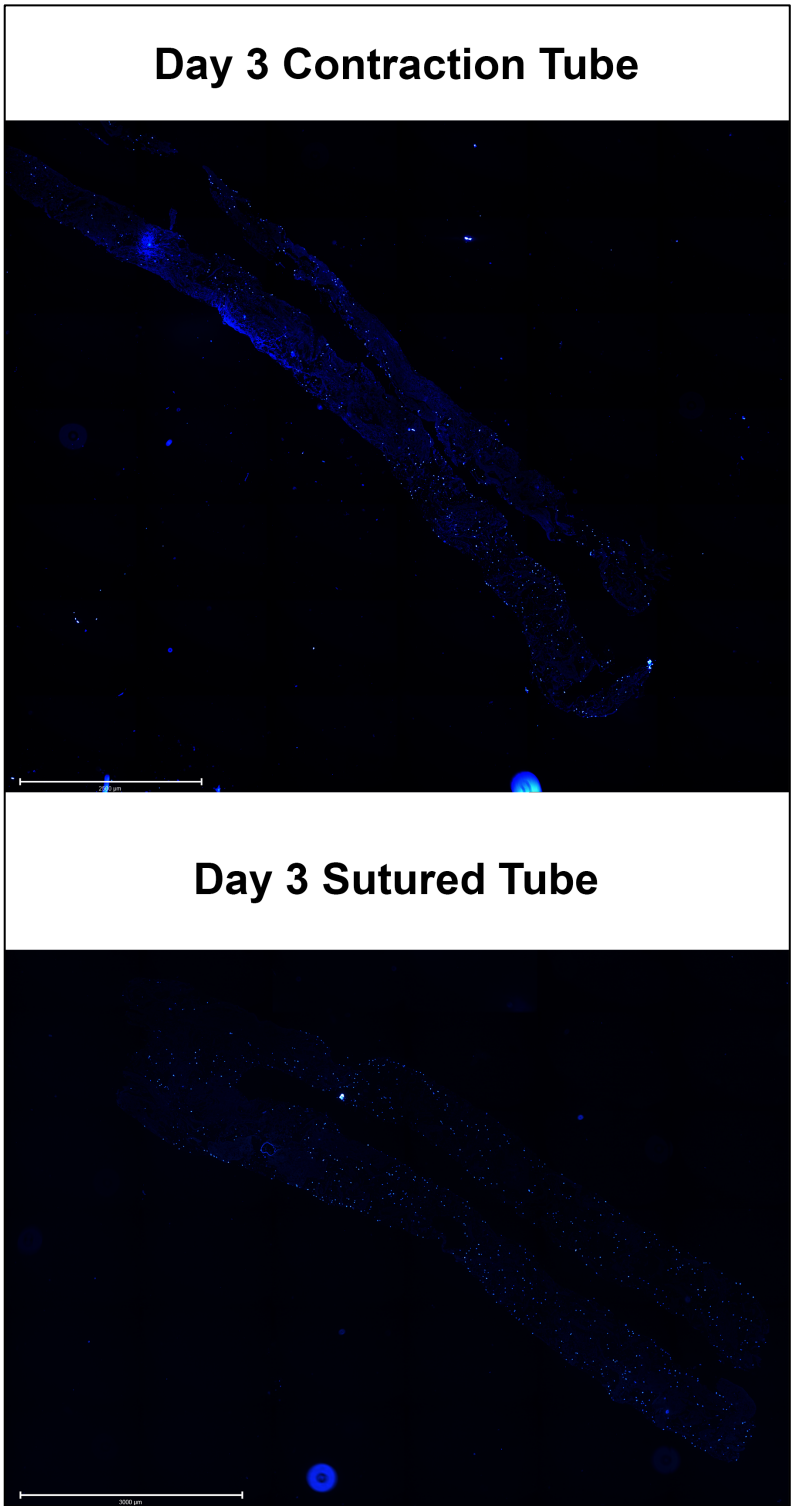

Figure 3.2 Cytotubes sutured within bioreactors displayed more even cellular distribution as indicated by the cell nuclei (DAPI) on day 3 than those that were subjected to static petri dish cultures. The day 3 contraction tube showed fewer cells in the middle region of the tube, but more cells were clustered near the ends of the tube as indicated by relative blue staining intensity.

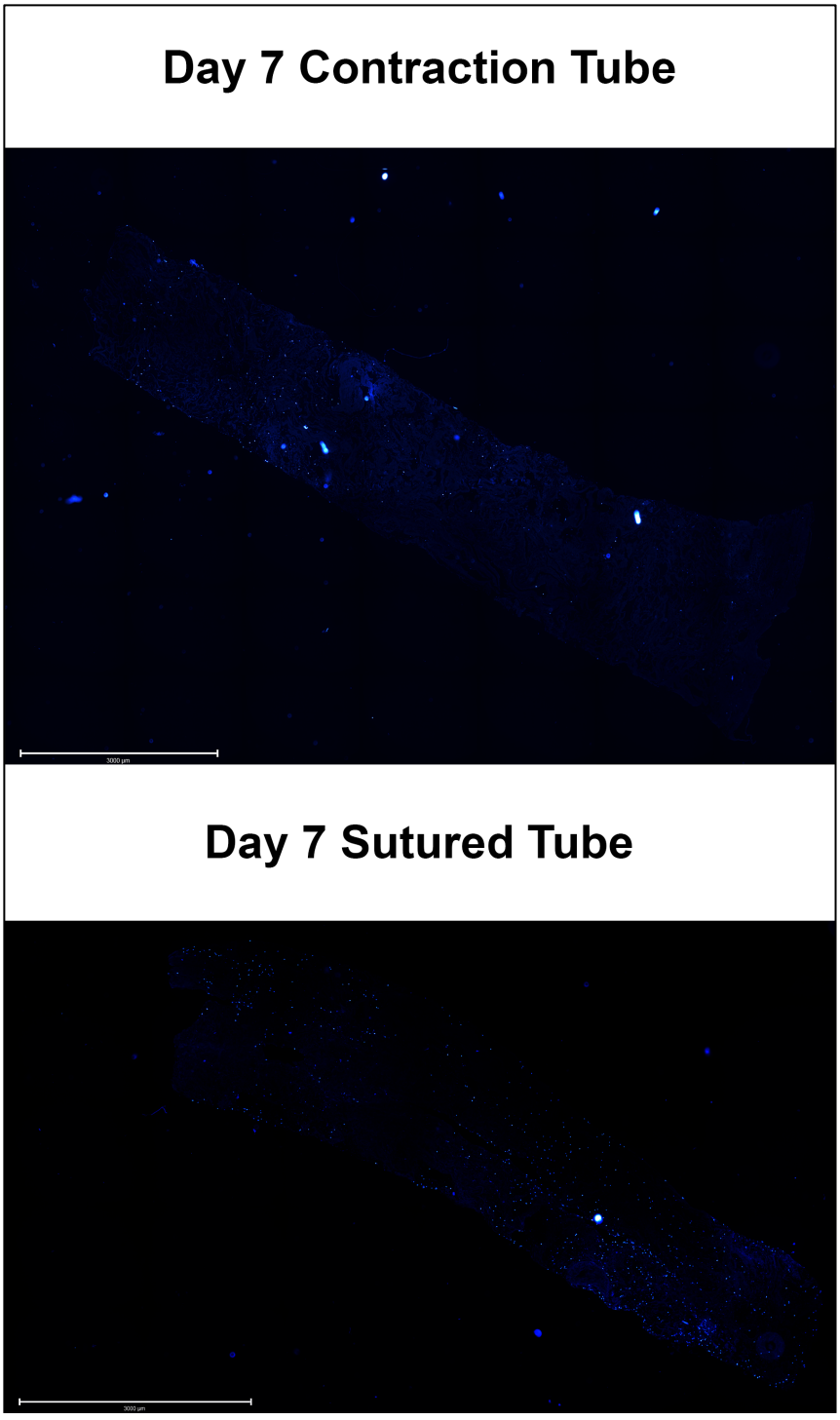

Figure 3.3 According to relative blue staining intensity, SMCs in day 7 cytotubes that were cultured under static petri dish cultures without sutures were gathered more on one end of the tube whereas the SMCs that were cultured with sutures in bioreactors still maintain very even cellular distribution throughout the entire tube geometry.

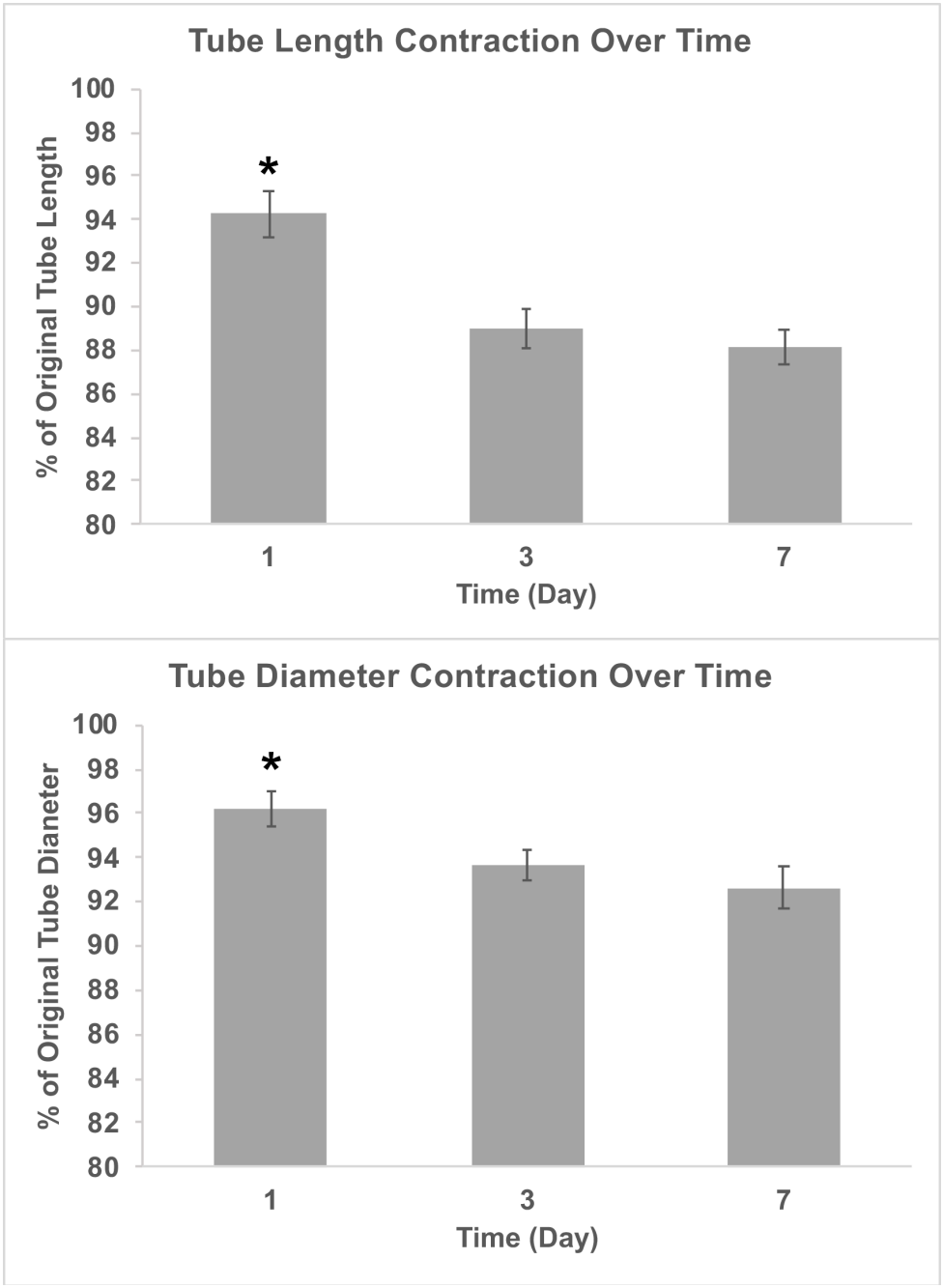

Figure 3.4 Cytotube length and diameter contraction varied over time. The analyses of tube contraction for length (top) and outer diameter (bottom), respectively, were plotted as mean ± SEM. SMC-only cytotubes cultured without sutures in petri dishes showed a high level of shrinkage for length, measuring at 88.12 ± 0.82% of the original tube length and 92.64 ± 0.94% of the original tube diameter after seven days of culture. For $p<0.05$, mean differences of contraction were found to be significant between Day 1 and 3 and Day 1 and 7 for both tube length and diameter (as indicated by the asterisks).

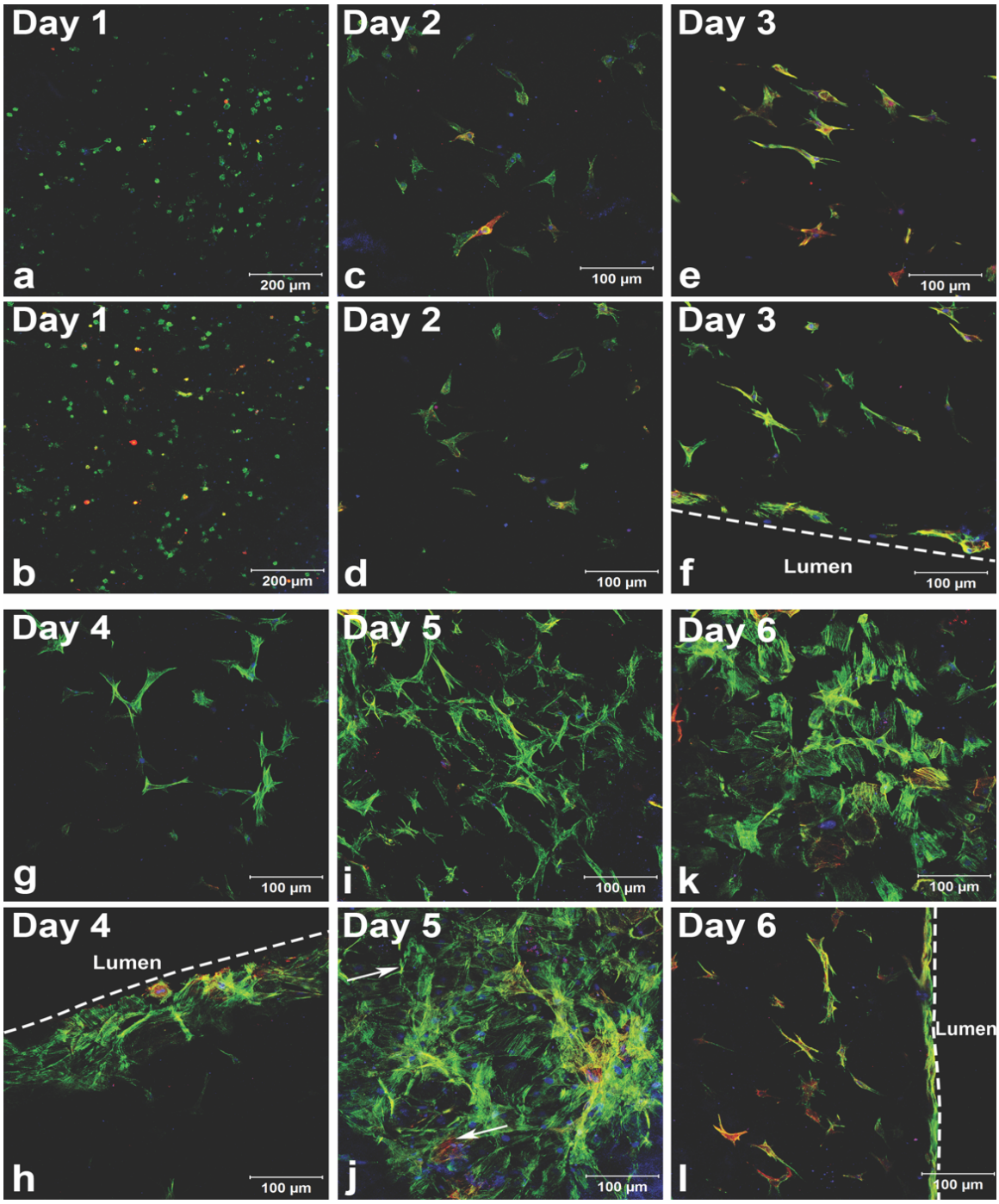

Figure 3.5 Fibroblasts (FBs) cast within the cytotube wall were initially spherical in shape throughout the entire construct (a,b) but over time adopted different morphologies specific to their location within the cytotube. FBs within the wall exhibited early (c,d) and more exaggerated (e,g) stellate morphologies, typical of mesenchymal cells, with densely associated layers of FBs in later time points (i,k). In contrast, FBs near the luminal surface aligned along the wall edge with increased f-actin expression based on green staining intensity (f,h) and flattened squamous morphology in epithelial-like organization (j,l). Numerous intracellular

stress fibers (j, top arrow) and organized α smooth muscle actin filaments (red staining, j, bottom arrow) were visible along with cell nuclei [4′6-diamidino-2-phenylindole (DAPI), blue staining].

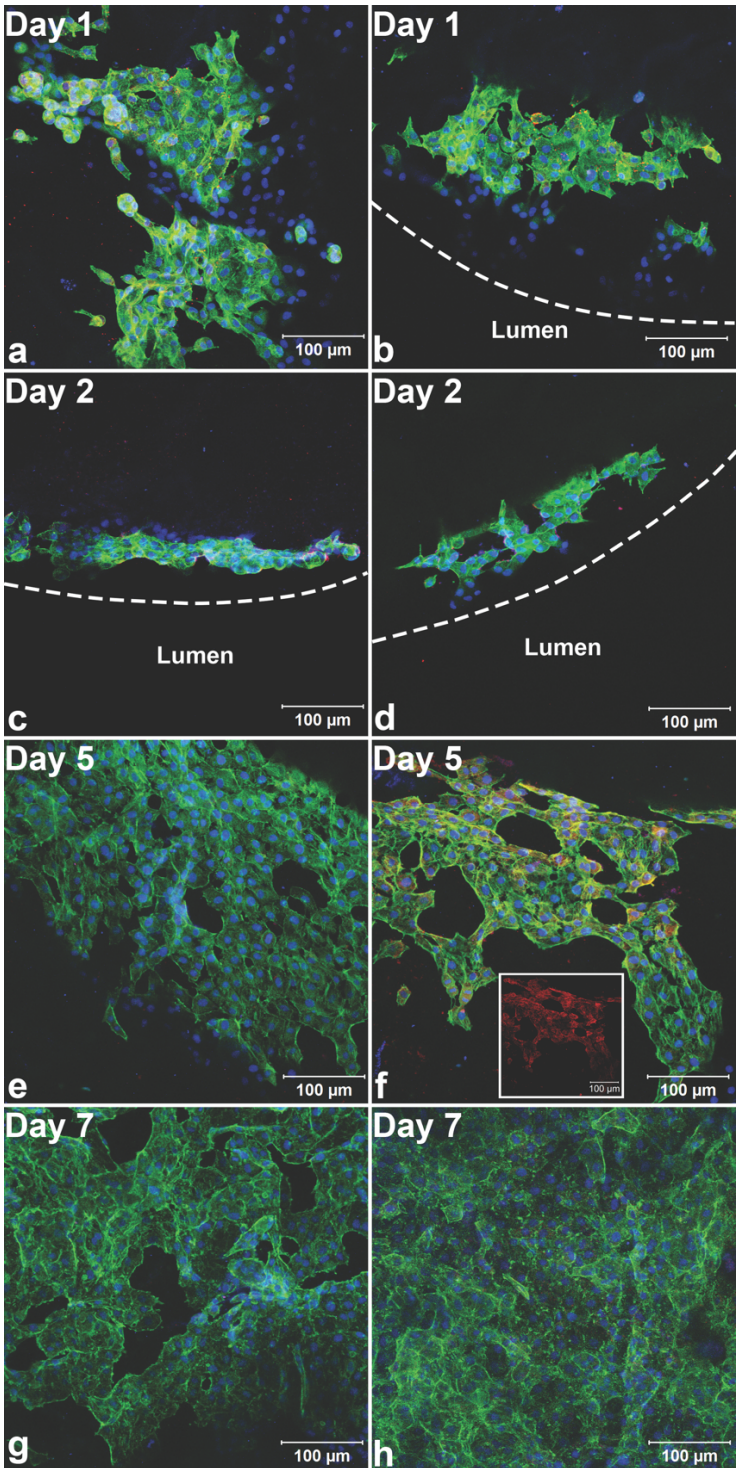

Figure 3.6 Endothelial cells (ECs) were seeded onto the luminal surfaces of cytotubes where small globular clusters of polygonal endothelial cells with associated f-actin networks (green staining) were initially observed (a,b). Extensive cortical arrangements of f-actin associated with adjacent ECs along the luminal boundary indicated the potential development of tight junctions between these cells (c,d). In later time points, some ECs had α smooth muscle actin

filaments (f, red staining) although most exhibited increasing confluency and squamous morphology (e,g,h). Cell nuclei are shown with blue staining [4′6-diamidino-2-phenylindole (DAPI)].

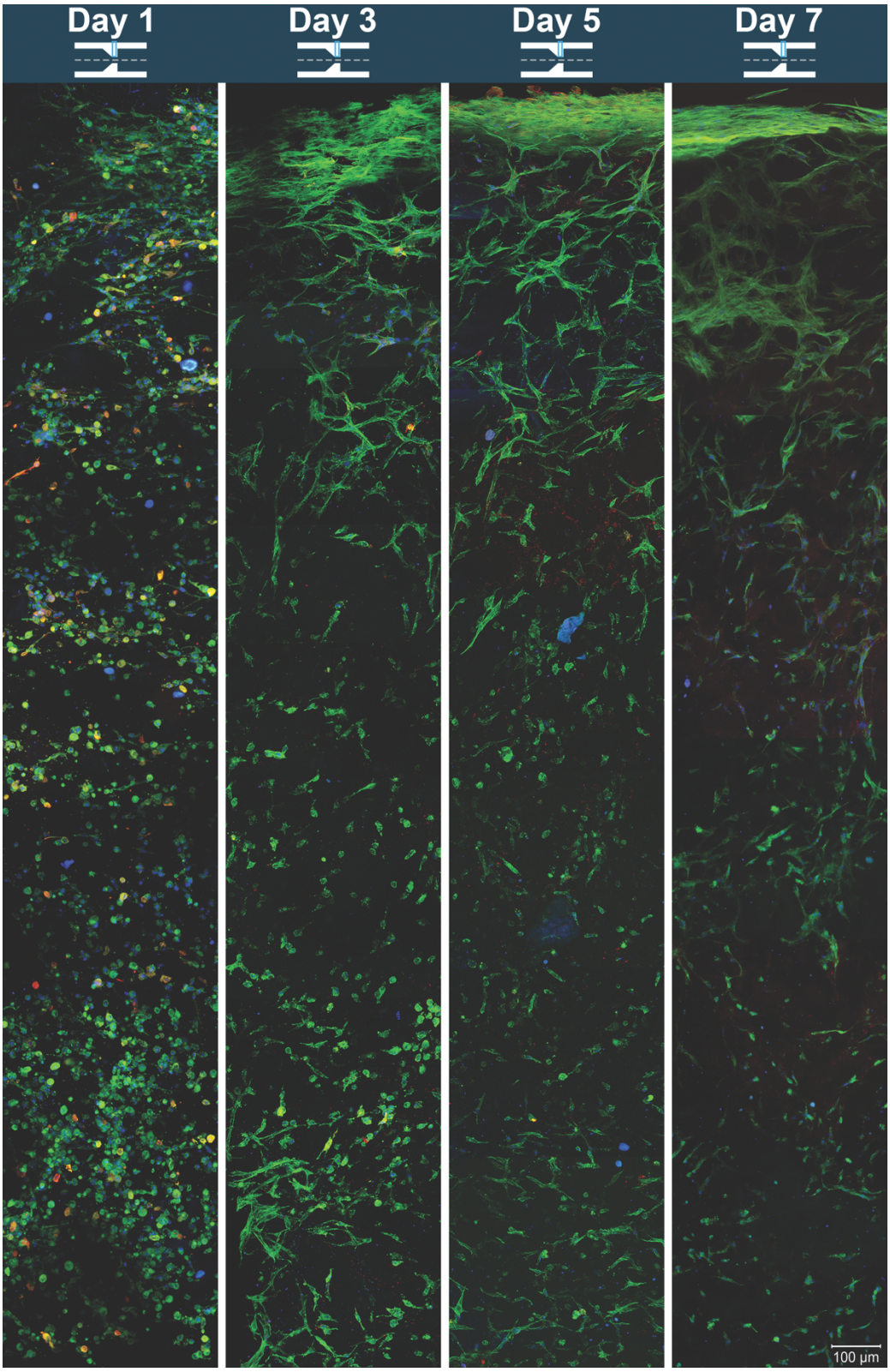

Figure 3.7 Vibratome sections of smooth muscle cells (SMC)-only cytotubes were stained for confocal microscopy, and the resulting images were collected and tiled

together. Representative sections from days 1, 3, 5, and 7 are shown in the four panels displayed from top to bottom that correspond to the exterior wall edge to the luminal edge, respectively. The schematic at the top of each panel depicts the geometry of the tube section and the area enclosed by the blue box represents the area displayed in the panel. Initially, spherical cells are observed throughout the construct. Fusiform SMCs can be seen on the luminal side in inter- mediate time points while stellate SMCs accumulate at the exterior wall in later time points. Green staining is f-actin, blue is 4′6-diamidino-2-phenylindole (DAPI), and red is α smooth muscle actin.

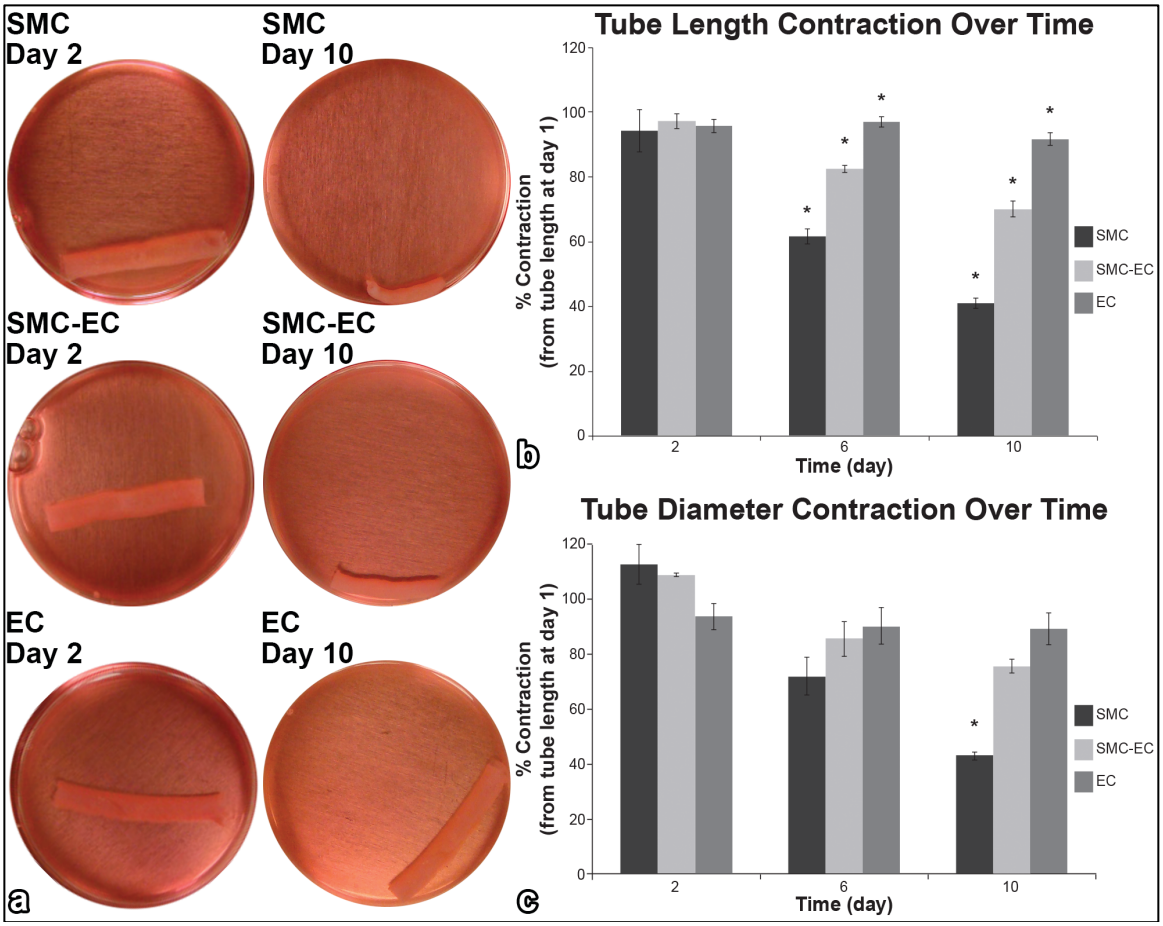

Figure 3.8 Cytotube length and diameter contraction varied with cell composition as shown in representative images of cytotube contraction over time (a). The analyses of tube contraction for length (b) and outer diameter (c), respectively, were plotted as mean ± SEM. Smooth muscle cells (SMC)-only cytotubes showed the highest level of shrinkage for length (58.95 ± 1.6%) and diameter (56.81 ± 1.5%), followed by SMC-endothelial cells (EC) cytotubes with 29.95 ± 2.4% for length and 24.45 ± 2.5% for diameter. EC-only cytotubes showed almost no shrinkage in 10 days of static culture with decreases of 8.34 ± 2.1% in length and 11.05 ± 4.7% in diameter. For $p<0.05$, mean differences of contraction length were found to be significant between all culture types for day 6 and 10, while mean differences of contraction diameter were found to be significant only at day 10 for SMC versus SMC-EC and SMC versus EC (as indicated by asterisks).

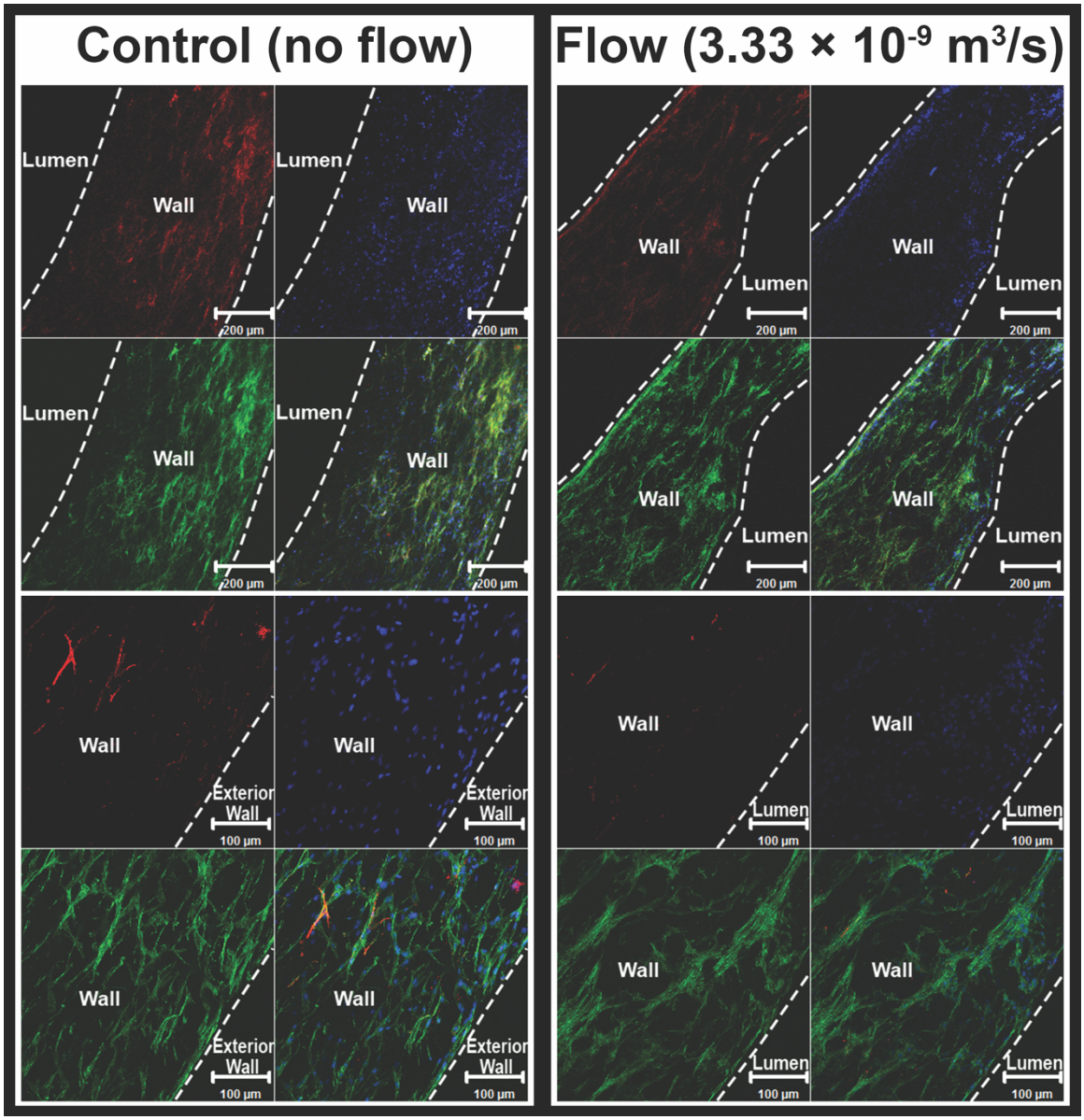

Figure 3.9 Static and dynamic culturing of cytotubes was performed with fluid flow bioreactors. The two left panels are representative images of cytotubes containing fibroblasts (FBs) and bone marrow primary cells (BMPCs) that were attached to bioreactors with no flow applied. The two panels on the right are representative images of FB-BMPC cytotubes cultured on bioreactors connected to pumps with an applied flow rate of 3.33×10^{-9} m^3/s of culture media through the tube lumen. Both types of cytotubes were cultured for 48 h. Cytotubes cultured with flow showed increased alignment of cells and α smooth muscle actin (red staining) compared with control samples. Green staining is f-actin and blue is 4′6-diamidino-2-phenylindole (DAPI).

CHAPTER 4

DISCUSSION AND CONCLUSIONS[4]

4.1 CYLINDRICAL CYTOTUBE DISCUSSION

4.1.1 Cylindrical Cytotube Discussion

We have previously developed numerous models of three-dimensional in vitro systems using collagen as the principle material in order to simulate biological processes.[27,29,30,38,39] Very little is known about how cells reorganize and align themselves in 3D environments where there are two extremes: vascular cells under tension and cells that are free to restructure their environment at will without the interference of outside sources.[40,4142] Experiments were carried out to examine the effect of cellular tension on vascular smooth muscle cells in these 3D collagen gels by culturing cylindrical cytotubes in static petri dishes with no attachments and in bioreactors mounted with sutures without applied flow.

Immunofluorescent staining proved to be challenging with these constructs, however the reasons for this are still unknown and warrant further study. While it is possible that paraffin-embedding could have created the barriers in staining, it is unlikely given that DAPI proved to have viable staining results. Analysis of the

[4] Parts of this chapter have been excerpted from the following research article:

1. Jones RS, Chang PH, Perahia T, et al. Design and Fabrication of a Three-Dimensional in Vitro System for Modeling Vascular Stenosis. *Microsc Microanal*. 2017;23(4):859-871. doi:10.1017/S1431927617012302

EVOS images using DAPI to delineate cellular distribution illustrated differences in cellular alignment within the sutured and non-sutured collagen tubes. Over seven days of culture, cylindrical cytotubes that were sutured in bioreactors maintained even cellular distribution as indicated by blue staining from DAPI for cellular nuclei. After three days of culture, cells in non-sutured cytotubes showed more cellularization at either end of the tube with fewer cells in the middle. This could perhaps indicate that cells were migrating as a result of some stimuli or that they were dying. Further analysis and staining for f-actin as well as other SMC markers would provide more clarification. Following seven days of culture, cytotubes without sutures had far more cellularization at one end of the tube than the other. Again, this warrants more staining for a conclusive explanation as to the phenomena, however it is very evident that cytotubes with sutures displayed even cellular distribution in both Day 3 and Day 7 samples, suggesting that cellular tension does play a role in cellular reorganization within type I collagen martrices.

Contraction analysis showed these cylindrical cytotubes decreased in both length and diameter when statically cultured without tension added by sutures. While contraction for both length and diameter were significant between Day 1 and Day 3 and between Day 1 and Day 7, neither contraction amount was significant between Day 3 and Day 7 for length or diameter. This result could suggest that by Day 3, the majority of the cells have reorganized and restructured the 3D collagen environment to their satisfaction; thus, there is no need for more contraction if the SMCs are at optimal tension within the 3D matrix.[12] This assertion would also

necessitate further research and confirmation with staining for specific cell markers and PCR.

4.2 VASCULAR STENOSIS DISCUSSION

4.2.1 Vascular Stenosis Discussion

Vascular stenosis can develop from numerous conditions or pathologies at any stage of life and often provokes significant detrimental consequences to cardiovascular health.[5–7] Despite increasing prevalence and mortality due to cardiovascular diseases associated with vascular stenosis, a sufficient artery model that can be used to examine and define the mechanism in which these pathologies occur has yet to be developed; hence, the roles that specific molecules, cells, environments, and hemodynamic stimuli play in the events that lead to the progression of these conditions are not clearly understood.[20,21,31]

The lack of complexity offered by standard two-dimensional cell cultures is analogous to the convoluted results of in vivo studies that, due to natural variation and the multifaceted system of responses in the body, cannot be conclusively analyzed and interpreted. The paucity of adequate systems for the study of vascular diseases and engineered tissues has elicited a strong demand for intermediate levels of complexity in research models while also serving as a motivation for these studies. A number of vascular biofabrication methodologies have been developed prior to this investigation, however few have incorporated cells into the vascular wall and in the lumen as seen in this study.[22,43–49] Here, two processes, cellularized collagen wall casting and rotator-assisted luminal cell seeding, were developed to generate cellularized tubes or “cytotubes” with several

different combinations of cells within the collagen wall and in the tube lumen. The casting of the cellularized collagen wall required a protocol to be designed in which the requisite pH shift for collagen polymerization was carried out while maintaining cell viability. This polymerization technique allowed us to produce cellularized collagen tubes serving as arterial scaffolds that can be cultured to allow morphological adaptation under conditions of applied flow or static culture. From this, we created a construct with a stenotic luminal geometry that, under dynamic flow conditions, can be used to generate areas of disturbed flow while also exposing cells in the lumen and the wall of the cytotube to mechanical stimuli from the force of the applied flow.[17] While future studies involving further manipulation and analysis of the applied flow and its effects are required to achieve conditions similar to the in vivo environment, our cytotubes coupled with the dynamic bioreactor culture systems present a unique innovative method for gaining insight into vascular pathology.

In general, the processes that regulate the transduction of mechanical stimuli into cellular activities are not well characterized.[50] In the case of arterial stenosis, the narrowed lumen alters hemodynamics, including blood flow rate and pressure, hence the overall mechanical environment of vascular cells is directly affected.[7,20] More specifically, the process by which this altered environment impacts cellular processes such as endothelial activation, smooth muscle cell proliferation, and pathological ECM remodeling is not clear.[6,7,21] The signaling between cells of the intima, media, and adventitia is likely, if not required, to be coordinated during pathological progression, hence the presence of more than one

representative vascular cell type in models of vascular disease is essential.[20] Delineating these mechanisms offers the opportunity to intervene therapeutically at a number of clinically relevant stages of disease progression, essentially from prevention to regeneration.

To accommodate the presence of more than one vascular cell type in our preliminary model of vascular stenosis, we developed our techniques for luminal cell seeding in combination with the cellularized wall casting, which allowed for the generation of cytotubes containing cells within the collagen wall and in the tube lumen as seen with our SMC-EC co-culture cytotubes. To investigate the effects of seeding cytotubes with different cell types, we compared SMC-only, EC-only, and SMC-EC cytotubes in static culture and measured dimensional changes in tube diameter and length over time. This study found that the SMC-EC cytotubes behaved differently than either EC- or SMC-only constructs, taking on an intermediate tube contraction phenotype in both length and diameter. Adding complexity to this system offers the opportunity to determine the various roles of interactions between resident vascular cells and the immune cells that are thought to drive pathological remodeling of the vessel tissue.

One of the most notable phenomena observed with our system was the increasingly uneven dispersion of SMCs within the tube wall and the increasing cellularity of SMCs at and near the outer surfaces of the cytotube over time (Fig. 6). While this observation can also be considered a limitation of our system, future studies are planned to investigate this as it is not clear whether cells within the wall migrate toward the surfaces, die at higher rates between the surfaces, or whether

surface-dwelling cells proliferate at higher rates. SMCs are reported to proliferate in response to pressure[51]; thus, it would be interesting to carry out these studies in a system of variable pressure in order to determine how this affects SMC density and distribution. Though our initial flow experiments with cytotubes fabricated with FBs and BMPCs revealed only a few prominent differences from no-flow cultures, future experiments using different parameters will investigate this further. The initial result is not surprising since flow is typically sensed by lumen-lined EC, which were not present in that particular experiment; however, it is known that in the event of EC denudation, adventitial FBs migrate and contribute to neointima formation.[20] In addition, it has been reported that minor increases in interstitial flow, which is flow that permeates through the vascular wall and is much lower than the flow levels typically sensed by ECs, can promote FB migration.[20,52,53] Although interstitial flow rates were not calculated in this study, it is possible that the increase in cellular alignment along the wall edges, in cytotubes cultured with flow, could be a result of the applied flow rate promoting FB motility. The lack of extensive distinct characteristics in flow and no-flow tubes may also be attributed to the low, creeping level of flow or the lack of applied pressure under which those samples were cultured. This creeping flow rate was intentionally chosen because it resulted in minimal pressure levels compared with conditions in vivo, which was an integral step in discerning the effects of flow rather than pressure and flow combined on the vascular environment. The normal complementary relationship between blood flow rate and pressure is disrupted in vascular stenosis; hence these components and their effects should be evaluated separately and together. Further

experimentation is necessary to determine the extent of the influence from the creeping flow and low pressure factors and if differences exist between the proximal, stenotic, or distal sections of the cytotube.

4.3 CYLINDRICAL CYOTUBE AND VASCULAR STENOSIS CONCLUSIONS

Using a unique fabrication approach that allows for polymerization of collagen while maintaining cell viability, we have created and cultured cellularized tubes with cylindrical geometry and stenotic luminal geometry that support the growth and morphogenesis of resident vascular cell types. Furthermore, these stenotic constructs were coupled with a fluid flow bioreactor to investigate the effects of low, creeping flow through the tube lumen. Future investigations involving cytotubes cultured in bioreactors can provide more insight into the hemodynamic forces and interactions with the tissue that drive developmental and pathological processes. Imminent endeavors for this research include: co-culturing cytotubes with more than two cell types; varying the flow properties and hemodynamic stimuli for bioreactor cultures and developing cytotubes with different geometries to generate disturbed flow. Co-culturing the three characteristic vascular cell types together, ECs, SMCs, and FBs, could potentially produce dramatically different results with regards to cellular position and dispersion, ECM development, and other organizational trends. Altering the geometries of the cytotubes would also help to define specific cellular responses to disturbed flow in a region-specific manner. Lastly, further use of the bioreactors for culturing tubes under steady flow or conditions more similar to the in vivo environment can help to delineate some of the cellular responses to specific

mechanical stimuli. Our novel fabrication processes with the versatile culturing system offer a substantial approach with extensive potential to make a contribution to the field of research for vascular disease and tissue engineering.

REFERENCES

1. Li DY, Toland AE, Boak BB, et al. Elastin point mutations cause an obstructive vascular disease, supravalvular aortic stenosis. *Hum Mol Genet*. 1997;6(7):1021-1028. doi:10.1093/hmg/6.7.1021
2. Williams JCP, Barratt-Boyes BG, Lowe JB. Supravalvular aortic stenosis. *Circulation*. 1961;24(6):1311-1318. doi:10.1161/01.CIR.24.6.1311
3. Thiriet M, Delfour M, Garon A. Vascular stenosis: An introduction. In: Lanzer P, ed. *PanVascular Medicine*. 2nd ed. Berlin, Heidelberg: Springer Berlin Heidelberg; 2015:781-868. doi:10.1007/978-3-642-37078-6_32
4. McElhinney DB, Parry AJ, Reddy VM, Hanley FL, Stanger P. Left pulmonary artery kinking caused by outflow tract dilatation after transannular patch repair of tetralogy of Fallot. *Ann Thorac Surg*. 1998;65(4):1120-1126. doi:http://dx.doi.org/10.1016/S0003-4975(98)00112-X
5. Galis ZS, Khatri JJ. Matrix metalloproteinases in vascular remodeling and atherogenesis: the good, the bad, and the ugly. *Circ Res*. 2002;90(3):251-262. http://www.ncbi.nlm.nih.gov/pubmed/11861412. Accessed January 6, 2015.
6. Chiu J-J, Chien S. Effects of disturbed flow on vascular endothelium: pathophysiological basis and clinical perspectives. *Physiol Rev*. 2011;91(1):327-387. doi:10.1152/physrev.00047.2009

7. Kwak BR, Bäck M, Bochaton-Piallat M-L, et al. Biomechanical factors in atherosclerosis: mechanisms and clinical implications. *Eur Heart J*. 2014;35(43):3013-3020. doi:10.1093/eurheartj/ehu353

8. NIH, NHLBI. Chapter 4 Disease Statistics. In: *NHLBI Fact Book, Fiscal Year 2012*. ; 2012:33-52. https://www.nhlbi.nih.gov/about/factbook/chapter4.htm#gr36. Accessed March 24, 2014.

9. Malek AM. Hemodynamic Shear Stress and Its Role in Atherosclerosis. *JAMA*. 1999;282(21):2035. doi:10.1001/jama.282.21.2035

10. Chatzizisis YS, Coskun AU, Jonas M, Edelman ER, Feldman CL, Stone PH. Role of endothelial shear stress in the natural history of coronary atherosclerosis and vascular remodeling: molecular, cellular, and vascular behavior. *J Am Coll Cardiol*. 2007;49(25):2379-2393. doi:10.1016/j.jacc.2007.02.059

11. Ross R. Atherosclerosis--an inflammatory disease. *N Engl J Med*. 1999;340(2):115-126. doi:10.1056/NEJM199901143400207

12. Gimbrone MA, García-Cardeña G. Vascular endothelium, hemodynamics, and the pathobiology of atherosclerosis. *Cardiovasc Pathol*. 2013;22(1):9-15. doi:10.1016/j.carpath.2012.06.006

13. Ku DN, Giddens DP, Zarins CK, Glagov S. Pulsatile flow and atherosclerosis in the human carotid bifurcation. Positive correlation between plaque location and low oscillating shear stress. *Arterioscler Thromb Vasc Biol*. 1985;5(3):293-302. doi:10.1161/01.ATV.5.3.293

14. Tarbell JM, Shi Z-D, Dunn J, Jo H. Fluid Mechanics, Arterial Disease, and Gene Expression. *Annu Rev Fluid Mech*. 2014;46(1):591-614. doi:10.1146/annurev-fluid-010313-141309

15. Holzapfel GA, Gasser TC, Ogden RW. A New Constitutive Framework for Arterial Wall Mechanics and a Comparative Study of Material Models. *J Elast Phys Sci solids*. 2000;61(1-3):1-48. doi:10.1023/A:1010835316564

16. Eberth JF, Popovic N, Gresham VC, Wilson E, Humphrey JD. Time course of carotid artery growth and remodeling in response to altered pulsatility. *Am J Physiol Heart Circ Physiol*. 2010;299(6):H1875-H1883. doi:10.1152/ajpheart.00872.2009

17. Eberth JF, Gresham VC, Reddy AK, Popovic N, Wilson E, Humphrey JD. Importance of pulsatility in hypertensive carotid artery growth and remodeling. *J Hypertens*. 2009;27(10):2010-2021. doi:10.1097/HJH.0b013e32832e8dc8

18. Libby P, Ridker PM, Hansson GK. Progress and challenges in translating the biology of atherosclerosis. *Nature*. 2011;473(7347):317-325. doi:10.1038/nature10146

19. Heusch G, Libby P, Gersh B, et al. Cardiovascular remodelling in coronary artery disease and heart failure. *Lancet*. 2014;383(9932):1933-1943. doi:10.1016/S0140-6736(14)60107-0

20. Shi Z-D, Tarbell JM. Fluid flow mechanotransduction in vascular smooth muscle cells and fibroblasts. *Ann Biomed Eng*. 2011;39(6):1608-1619. doi:10.1007/s10439-011-0309-2

21. Libby P, Hansson GK. Inflammation and immunity in diseases of the arterial tree: players and layers. *Circ Res*. 2015;116(2):307-311. doi:10.1161/CIRCRESAHA.116.301313

22. Weinberg CB, Bell E. A blood vessel model constructed from collagen and cultured vascular cells. *Science*. 1986;231(4736):397-400. http://www.ncbi.nlm.nih.gov/pubmed/2934816. Accessed June 6, 2015.

23. Nerem RM, Ensley AE. The tissue engineering of blood vessels and the heart. *Am J Transplant*. 2004;4:36-42. doi:10.1111/j.1600-6135.2004.0343.x

24. Norris RA, Damon B, Mironov V, et al. Periostin regulates collagen fibrillogenesis and the biomechanical properties of connective tissues. *J Cell Biochem*. 2007;101(3):695-711. doi:10.1002/jcb.21224

25. Valarmathi MT, Yost MJ, Goodwin RL, Potts JD. A three-dimensional tubular scaffold that modulates the osteogenic and vasculogenic differentiation of rat bone marrow stromal cells. *Tissue Eng Part A*. 2008;14(4):491-504. doi:10.1089/tea.2007.0235

26. Evans HJ, Sweet JK, Price RL, Yost M, Goodwin RL. Novel 3D culture system for study of cardiac myocyte development. *Am J Physiol Heart Circ Physiol*. 2003;285(2):H570-H578. doi:10.1152/ajpheart.01027.2002

27. Yost MJ, Baicu CF, Stonerock CE, et al. A novel tubular scaffold for cardiovascular tissue engineering. *Tissue Eng*. 2004;10(1-2):273-284. doi:10.1089/107632704322791916

28. Valarmathi MT, Goodwin RL, Fuseler JW, Davis JM, Yost MJ, Potts JD. A

3-D cardiac muscle construct for exploring adult marrow stem cell based myocardial regeneration. *Biomaterials*. 2010;31(12):3185-3200. doi:10.1016/j.biomaterials.2010.01.041

29. Tan H, Biechler S, Junor L, et al. Fluid flow forces and rhoA regulate fibrous development of the atrioventricular valves. *Dev Biol*. 2013;374(2):345-356. doi:10.1016/j.ydbio.2012.11.023

30. Biechler S V, Junor L, Evans AN, et al. The impact of flow-induced forces on the morphogenesis of the outflow tract. *Front Physiol*. 2014;5:225. doi:10.3389/fphys.2014.00225

31. Mammoto T, Mammoto A, Ingber DE. Mechanobiology and developmental control. *Annu Rev Cell Dev Biol*. 2013;29:27-61. doi:10.1146/annurev-cellbio-101512-122340

32. Hahn C, Schwartz MA. Mechanotransduction in vascular physiology and atherogenesis. *Nat Rev Mol Cell Biol*. 2009;10(1):53-62. doi:10.1038/nrm2596

33. Valarmathi MT, Davis JM, Yost MJ, Goodwin RL, Potts JD. A three-dimensional model of vasculogenesis. *Biomaterials*. 2009;30(6):1098-1112. doi:10.1016/j.biomaterials.2008.10.044

34. Sung KE, Su G, Pehlke C, et al. Control of 3-dimensional collagen matrix polymerization for reproducible human mammary fibroblast cell culture in microfluidic devices. *Biomaterials*. 2009;30(27):4833-4841. doi:10.1016/j.biomaterials.2009.05.043

35. Achilli M, Mantovani D. Tailoring mechanical properties of collagen-based

scaffolds for vascular tissue engineering: the effects of pH, temperature and ionic strength on gelation. *Polymers (Basel)*. 2010;2(4):664-680. doi:10.3390/polym2040664

36. Azuma K, Ichimura K, Mita T, et al. Presence of alpha-smooth muscle actin-positive endothelial cells in the luminal surface of adult aorta. *Biochem Biophys Res Commun*. 2009;380(3):620-626. doi:10.1016/j.bbrc.2009.01.135

37. van Meeteren LA, ten Dijke P. Regulation of endothelial cell plasticity by TGF-β. *Cell Tissue Res*. 2012;347(1):177-186. doi:10.1007/s00441-011-1222-6

38. Jones RS, Chang PH, Perahia T, et al. Design and Fabrication of a Three-Dimensional in Vitro System for Modeling Vascular Stenosis. *Microsc Microanal*. 2017;23(4):859-871. doi:10.1017/S1431927617012302

39. Valarmathi MT, Yost MJ, Goodwin RL, Potts JD. The influence of proepicardial cells on the osteogenic potential of marrow stromal cells in a three-dimensional tubular scaffold. *Biomaterials*. 2008;29(14):2203-2216. doi:10.1016/j.biomaterials.2008.01.025

40. Huang AH, Balestrini JL, Udelsman B V, et al. Biaxial Stretch Improves Elastic Fiber Maturation, Collagen Arrangement, and Mechanical Properties in Engineered Arteries. *Tissue Eng Part C Methods*. 2016;22(6):524-533. doi:10.1089/ten.TEC.2015.0309

41. Niklason LE. Understanding the Extracellular Matrix to Enhance Stem Cell-Based Tissue Regeneration. *Cell Stem Cell*. 2018;22(3):302-305.

doi:10.1016/J.STEM.2018.02.001

42. Zhang S, Cao X, Stablow AM, Shenoy VB, Winkelstein BA. Tissue Strain Reorganizes Collagen With a Switchlike Response That Regulates Neuronal Extracellular Signal-Regulated Kinase Phosphorylation In Vitro: Implications for Ligamentous Injury and Mechanotransduction. *J Biomech Eng*. 2016;138(2):021013. doi:10.1115/1.4031975

43. Kanda K, Matsuda T, Oka T. In vitro reconstruction of hybrid vascular tissue. Hierarchic and oriented cell layers. *ASAIO J*. 1993;39(3):M561-M565. http://www.ncbi.nlm.nih.gov/pubmed/8268599. Accessed September 8, 2015.

44. L'Heureux N, Germain L, Labbé R, Auger FA. In vitro construction of a human blood vessel from cultured vascular cells: a morphologic study. *J Vasc Surg*. 1993;17(3):499-509. doi:10.1016/0741-5214(93)90150-K

45. L'Heureux N, Pâquet S, Labbé R, Germain L, Auger FA. A completely biological tissue-engineered human blood vessel. *FASEB J*. 1998;12(1):47-56. http://www.fasebj.org/content/12/1/47.long. Accessed September 3, 2015.

46. Hirai J, Kanda K, Oka T, Matsuda T. Highly oriented, tubular hybrid vascular tissue for a low pressure circulatory system. *ASAIO J*. 1994;40(3):M383-M388. http://www.ncbi.nlm.nih.gov/pubmed/8555543. Accessed September 8, 2015.

47. Kanda K, Matsuda T. In vitro reconstruction of hybrid arterial media with molecular and cellular orientations. *Cell Transplant*. 1994;3(6):537-545.

http://www.ncbi.nlm.nih.gov/pubmed/7881764. Accessed September 8, 2015.

48. Niklason LE, Gao J, Abbott WM, et al. Functional arteries grown in vitro. *Science*. 1999;284(5413):489-493. doi:10.1126/science.284.5413.489

49. Kakisis JD, Liapis CD, Breuer C, Sumpio BE. Artificial blood vessel: the Holy Grail of peripheral vascular surgery. *J Vasc Surg*. 2005;41(2):349-354. doi:10.1016/j.jvs.2004.12.026

50. Ingber DE. Tensegrity: the architectural basis of cellular mechanotransduction. *Annu Rev Physiol*. 1997;59:575-599. doi:10.1146/annurev.physiol.59.1.575

51. Devlin AM, Clark JS, Reid JL, Dominiczak AF. DNA synthesis and apoptosis in smooth muscle cells from a model of genetic hypertension. *Hypertension*. 2000;36(1):110-115. doi:10.1161/01.HYP.36.1.110

52. Ng CP, Swartz MA. Fibroblast alignment under interstitial fluid flow using a novel 3-D tissue culture model. *Am J Physiol Heart Circ Physiol*. 2003;284(5):H1771-H1777. doi:10.1152/ajpheart.01008.2002

53. Shi Z-D, Ji X-Y, Qazi H, Tarbell JM. Interstitial flow promotes vascular fibroblast, myofibroblast, and smooth muscle cell motility in 3-D collagen I via upregulation of MMP-1. *Am J Physiol Heart Circ Physiol*. 2009;297(4):H1225-H1234. doi:10.1152/ajpheart.00369.2009

54. Reller MD, Strickland MJ, Riehle-Colarusso T, Mahle WT, Correa A. Prevalence of Congenital Heart Defects in Metropolitan Atlanta, 1998-2005. *J Pediatr*. 2008;153(6):807-813. doi:10.1016/j.jpeds.2008.05.059

55. Bjornard K, Riehle-Colarusso T, Gilboa SM, Correa A. Patterns in the prevalence of congenital heart defects, metropolitan Atlanta, 1978 to 2005. *Birth Defects Res Part A Clin Mol Teratol*. 2013;97(2):87-94. doi:10.1002/bdra.23111

56. Midgett M, Thornburg KL, Rugonyi S. Blood flow patterns underlie developmental heart defects. *Am J Physiol - Hear Circ Physiol*. 2017;312(3):H632-H642. doi:10.1152/ajpheart.00641.2016

57. Dyer LA, Kirby ML. Sonic hedgehog maintains proliferation in secondary heart field progenitors and is required for normal arterial pole formation. *Dev Biol*. 2009;330(2):305-317. doi:10.1016/j.ydbio.2009.03.028

58. Hutson MR, Sackey FN, Lunney K, Kirby ML. Blocking hedgehog signaling after ablation of the dorsal neural tube allows regeneration of the cardiac neural crest and rescue of outflow tract septation. *Dev Biol*. 2009;335(2):367-373. http://www.ncbi.nlm.nih.gov/pubmed/19765571. Accessed November 20, 2017.

59. Waldo K, Zdanowicz M, Burch J, et al. A novel role for cardiac neural crest in heart development. *J Clin Invest*. 1999;103(11):1499-1507. doi:10.1172/JCI6501

60. Imanaka-Yoshida K, Hiroe M, Yoshida T. Interaction between cell and extracellular matrix in heart disease: multiple roles of tenascin-C in tissue remodeling. *Histol Histopathol*. 2004;19(2):517-525. doi:10.14670/HH-19.517

APPENDIX A

CONOTRUNCAL HEART DEFECTS: ALTERED TISSUE MORPHOLOGY AND HEMODYNAMICS[5]

Each year in the US, about 40,000 babies are born with congenital heart defects (CHDs).[54] While the array of causes of CHDs continues to widen and diversify, the prevalence of CHDs, especially the more common, less severe CHDs, is growing.[55] CHDs are known to be caused by genetic mutations and irregular hemodynamic forces during embryonic development; however, the cause of specific types of CHDs relative to these factors is much more obscure as many known aberrations in heart development produce a variable range of CHDs. Furthermore, the extent of the interaction between genetic and environmental components is an even more nebulous area of research.[56] To elucidate more information on the interplay between molecular and hemodynamic influences, we have utilized two different models of CHDs to analyze tissue morphology and create three-dimensional reconstructions of CHDs in order to predict hemodynamic properties. An avian model of Tetralogy of Fallot (TOF), characterized by ventricular septal defect, pulmonary obstruction (stenosis or

[5] Parts of this appendix were excerpted from the following research abstract:

1. Jones RS, Junor L, Hutson MR, Kirby ML, Goodwin RL. Conotruncal Heart Defects: Altered Tissue Morphology and Hemodynamics. *Microsc Microanal*. 2017;23(S1):1174-1175. doi:10.1017/S1431927617006535

atresia), overriding aorta, and right ventricular hypertrophy, has been developed through inhibition of Sonic hedgehog (Shh), which reduces proliferation of the secondary heart field (SHF). The Shh-null mouse was originally described as a phenotypic equivalent of TOF with pulmonary atresia as Shh is necessary for outflow tract (OFT), neural crest (NC) cell, and SHF proliferation. In previous studies, cyclopamine, an inhibitor of hedgehog signaling, decreased SHF proliferation and migration. Abnormal SHF proliferation has been linked to arterial pole defects, suggesting that cyclopamine treatment may yield arterial pole defects later in development.[57] Ablation of the NC has also been used as another avian model of CHDs that most commonly results in persistent truncus arteriosus (PTA) or other OFT malalignment defects such as double outlet right ventricle and TOF. NC ablation results in a failure of the SHF to contribute myocardium, which yields disrupted patterning of the arterial pole.[57]

A.1 MATERIALS AND METHODS

Stock cyclopamine was dissolved in 95% EtOH and diluted with PBS.[57,58] In the present study, cyclopamine-treated eggs were windowed at Hamburger Hamilton (HH) stage 14 to pipette 10 μL of cyclopamine (0.8 μg/μL) or PBS/EtOH (control) onto the embryo, then resealed with tape and incubated. Cyclopamine treatment at HH 14 coincides with the initial contribution of myocardium to the distal OFT by the SHF.[57] For neural crest-ablated eggs, a pulsed nitrogen/dye laser (VSL-377/DLM-110; Laser Science Inc., Newton, Massachusetts, USA) was used to ablate the NC cells from the midotic placode to the third somite of HH stage 8 chicken embryos.[59] These cells seed the 3rd, 4th, and 6th pharyngeal arches and

have been defined as the cardiac NC. For neural crest ablated embryos, eggs were windowed after 30 hours of incubation then the embryos were lightly stained with neutral red–impregnated agar and staged. At HH 42, eggs of both treatment types were harvested, and the hearts and outflow vessels were fixed in either paraformaldehyde or glutaraldehyde then paraffin-embedded, sectioned (8 μm), and stained. H&E staining and Movat's pentachrome were used to analyze overall morphology (figure A.2), and staining with αSMA, collagen type I, tenascin, elastin, and DAPI was used for confocal microscopy.

Immunofluorescent labeling was used to identify cell phenotypes. All sections for confocal imaging were stained with fluorescently labeled 4′6-diamidino-2-phenylindole (DAPI, nuclear stain, no. D21490; Life Technologies, Carlsbad, CA, USA). One set of sections was stained with a rabbit anti-chicken collagen type I primary antibody (no. AB752P; EMD Millipore, Temecula, CA, USA), a goat anti-rabbit Alexa Fluor 488 secondary antibody (no. A11008; Life Technologies, Carlsbad, CA, USA), and an alpha smooth muscle actin (αSMA) antibody conjugated with Cy3 (no. C6198; Sigma-Aldrich, St. Louis, MO, USA). A second set of sections was stained with a rabbit anti-chicken tenascin primary antibody (no. AB19013; EMD Millipore, Temecula, CA, USA), a goat anti-rabbit Alexa Fluor 488 secondary antibody (no. A11008; Life Technologies, Carlsbad, CA, USA), and an alpha smooth muscle actin (αSMA) antibody conjugated with Cy3 (no. C6198; Sigma-Aldrich, St. Louis, MO, USA). A third set was stained with a rabbit polyclonal elastin primary antibody (no. AB21610; Abcam, Cambridge, MA, USA), a goat anti-rabbit Alexa Fluor 488 secondary antibody (no. A11008; Life

Technologies, Carlsbad, CA, USA), a mouse anti-chicken MF20 primary antibody (Developmental Studies Hybridoma Bank, Iowa City, IA, USA), and a donkey anti-mouse Alexa Fluor 546 secondary antibody (no. A10036; Life Technologies, Carlsbad, CA, USA). The sections were mounted on glass slides with 1,4-diazabicyclo[2.2.2]octane (DABCO, no. D2522; Sigma Aldrich, St. Louis, MO, USA) for confocal microscopy imaging (Zeiss LSM 510 Meta; Carl Zeiss, Thornwood, NY, USA).

AMIRA software was used to generate 3D models of myocardial and vessel tissue in addition to flow space from tiled serial sections of the heart and associated vessels.

A.2 RESULTS

At HH 42, the control, cyclopamine, and neural crest ablated (NCA) hearts were harvested from the chick embryos. Prior to harvesting, images were taken of the hearts to initially assess the overall structure of the hearts (Fig. A.1). Upon inspection, wide variations in outflow tract (OFT) vessel patterning were present in the cyclopamine and control hearts as compared to controls. In the normal chick hearts, the left and right brachiocephalic trunks and the aorta were shown to be originating from the left ventricle while the pulmonary trunks originated from the right ventricle (Fig. A.1 a-c). In Figure A.1 d, the pulmonary trunk was not visible, which would indicate complete pulmonary atresia, and there appeared to be an extra vessel originating from the aortic OFT. The cyclopamine heart in parts e and f also showed deviations in vessel patterning as compared to the control hearts. The NCA hearts in parts A.1g through A.1i possessed even more abnormal vessel

patterns, most of which indicated persistent truncus arteriosus, which is characterized by a common OFT.

In order to understand the vessel arrangement within the HH 42 hearts, the sectioned hearts were stained with Movat's pentachrome. Red staining indicates muscle, blue staining for ground substance and mucin, yellow for collagen fibers, and dark purple to black for nuclei and elastic fibers. In figure A.2, The control hearts in parts a and d had a well-defined aorticopulmonary septum (APS), which separates the aortic and pulmonary arteries. The APS of the cyclopamine heart in part e was very thin in comparison to that of the control hearts, while the other cyclopamine heart in part b and the NCA hearts in parts d through f lacked an APS entirely. In addition, the cyclopamine hearts had more ground substance based on blue staining intensity around the aorta and pulmonary vessels, which could indicate even more of an altered functionality in the muscle itself. The cyclopamine heart in part b was much smaller in overall size with what appeared to be a common outflow tract (OFT), however this was in fact complete pulmonary atresia, not PTA. The cyclopamine heart in part e also appeared to have a different shape compared to the control hearts as it was wider but more compact. The NCA hearts (c, f) demonstrated PTA and approximately four and a half leaflets in the main vessel of each heart. The NCA hearts were both noticeably smaller than the control hearts.

Confocal imaging was performed for the aortic and pulmonary vessels of the control and cyclopamine hearts as well as the common OFT of the NCA hearts. In Figure A.3, staining was done to show DAPI for cell nuclei and red for αSMA for

parts a through j. Parts a through e have green staining for collagen type I while parts f through j have green staining for tenascin, which is an ECM protein made by migrating cells like the neural crest during development.[60] The control aortas (a, f) showed a more uniform shape of the leaflets with smaller sinuses than in cyclopamine aortas. The cyclopamine aortas had more collagen type I overall (b) and αSMA (b, g) as indicated by their respective relative green and red staining intensities. The pulmonary vessels in the control hearts also had more collagen type I (c) and tenascin staining (h) in the valve leaflets than those in the cyclopamine hearts (d, j) based on relative staining intensity. The valve leaflets of the common OFTs in the NCA hearts (e, j) depicted more collagen type I and αSMA than both the aorta (a) and pulmonary vessels (c) in the control hearts.

Further confocal imaging was done using DAPI and elastin immunofluorescence staining in Figure A.4. The control aorta in part a depicted more presence of elastin than the cyclopamine aorta in part b as indicated by relative staining intensity. The DAPI staining for cell nuclei showed less cellularization and less elastin staining intensity in the control pulmonary leaflets (c) than those in the cyclopamine heart (d). More prominent elastin is shown around the common OFT of the NCA heart (e) than the aortic and pulmonary vessels in the control and cyclopamine hearts in parts a through d. The NCA heart also has leaflets that appeared to be the least cellularized overall as shown by relative blue staining intensity.

Figure A.5 shows AMIRA 3D reconstructions of serially sectioned hearts in order to get a better understanding of the anatomical structure of each heart and

its defects. The top row depicts the outer volume and vascular walls of control, cyclopamine, and NCA hearts. The bottom row depicts the flow space in each heart type. One cyclopamine heart shows pulmonary stenosis, which is classified as partial obstruction of the pulmonary vessel whereas the other cyclopamine heart illustrates pulmonary atresia, which is characterized as total obstruction of the lumen of the pulmonary vessel. The NCA heart is described as persistent truncus arteriosus. Variations in flow space and overall heart size are apparent.

A.3 DISCUSSION AND CONCLUSIONS

We have utilized two different models of CHDs to analyze tissue morphology and create three-dimensional reconstructions of CHDs in order to predict hemodynamic properties and to elucidate more information on the interplay between molecular and hemodynamic influences. We employed the avian model of TOF, characterized by ventricular septal defect, pulmonary obstruction (stenosis or atresia), overriding aorta, and right ventricular hypertrophy, through the inhibition of Sonic hedgehog (Shh), which reduces proliferation of the secondary heart field (SHF). Abnormal SHF proliferation has been linked to arterial pole defects, suggesting that cyclopamine treatment may yield arterial pole defects later in development.[57] Ablation of the NC was also used as another avian model of CHDs that most commonly resulted in persistent truncus arteriosus (PTA) or other OFT malalignment defects such as double outlet right ventricle and TOF.

Our results yielded a range of various cardiac malformations that showed drastic differences in overall tissue structure and morphology, which would indicate aberrations in hemodynamic function. We utilized a variety of methods to examine

the range of defects present in the cyclopamine-treated and NCA hearts including in vivo imaging, Movat's pentachrome staining, confocal imaging, and 3D AMIRA modeling. The pentachrome staining indicates substantial variation in collagen, ground substance, and muscle content throughout entire sections of the hearts. Confocal imaging defined areas with considerable differences in collagen type I, tenascin, and αSMA, which would imply altered tissue morphology and function. Finally, the AMIRA models allow visualization of those structural changes on a larger scale to provide insight on the hemodynamic changes that coincide with these specific cardiac malformations.

This novel approach for studying cardiac malformations during development has significant potential for providing further insight into the cause of these CHDs. While further investigation is needed, especially with volumetric analysis of the AMIRA models, we have created a unique system that allows for multiple levels of research into CHDs.

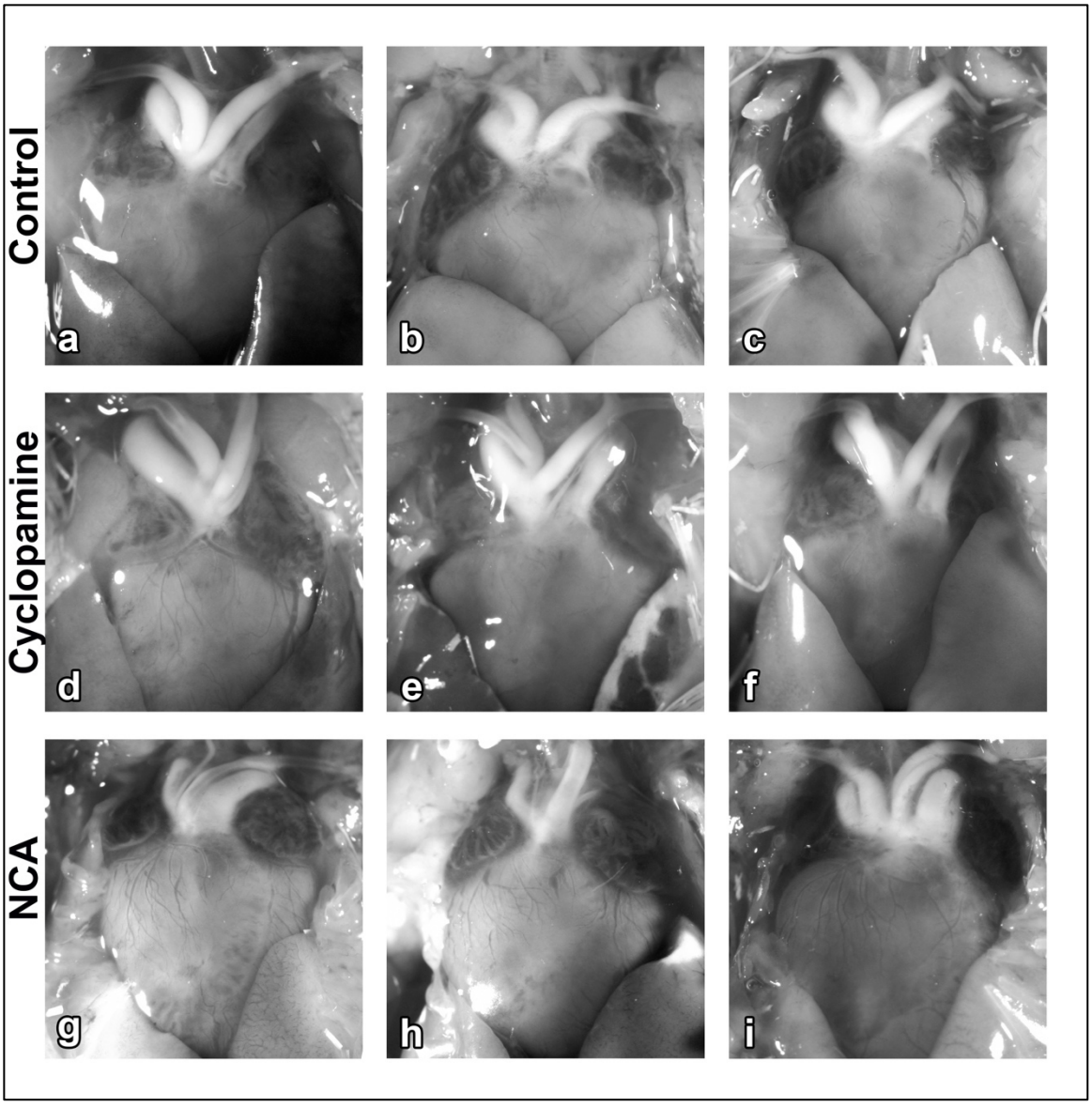

Figure A.1 shows the different vessel patterning for control, cyclopamine, and NCA hearts. The control hearts (a-c) demonstrate normal vessel patterns branching from the aorta and pulmonary arteries. The cyclopamine hearts show deviations from normal vessel patterns including complete pulmonary atresia (d) and pulmonary stenosis (e, f). The NCA hearts (g-i) all show PTA with varying numbers and arrangements of vessels branching out of the common OFT.

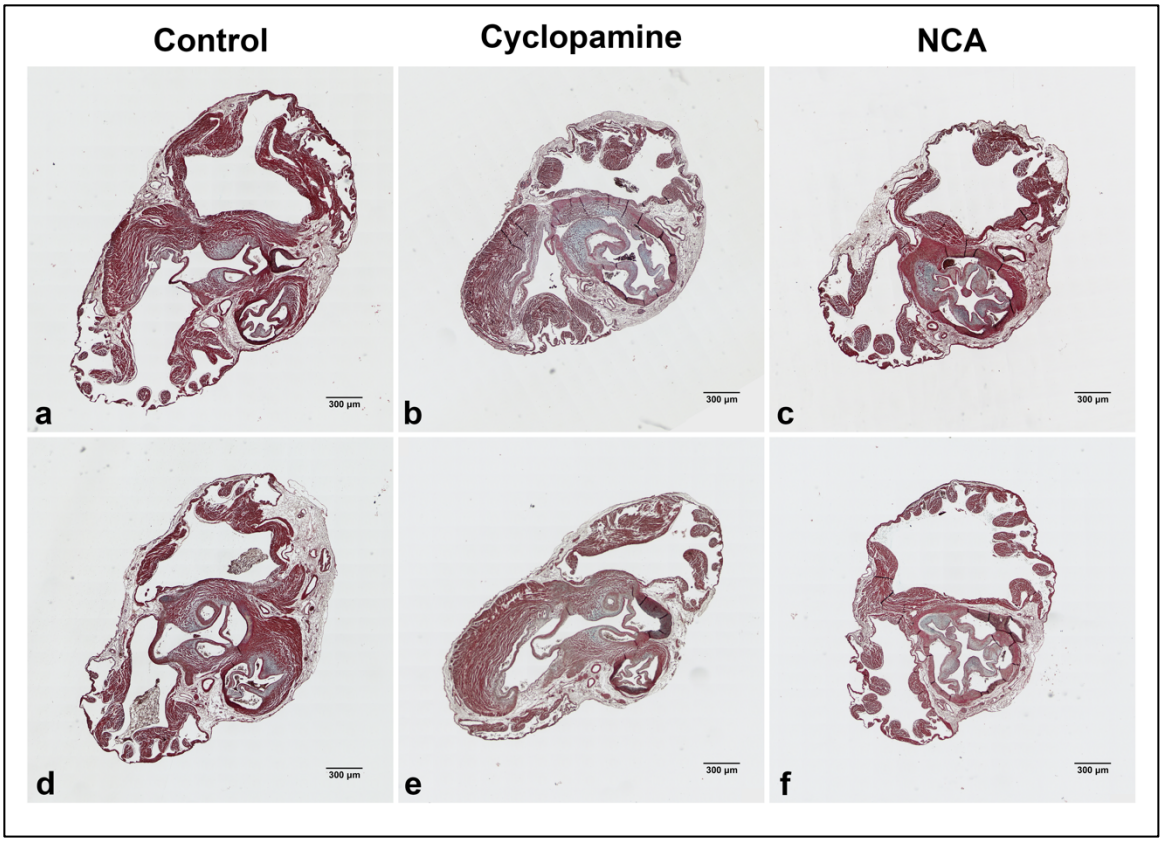

Figure A.2 is control, cyclopamine, and NCA hearts stained with Movat's Pentachrome. In general, the control hearts (a, d) have more red staining, indicating more muscle, and dark purple to black staining for elastic fibers than the cyclopamine and NCA hearts. The control hearts also have a well-defined aorticopulmonary septum (APS) in comparison to the thin, poorly muscularized APS in one cyclopamine heart (e) and the absence of the APSs in the NCA hearts (c, f) and the other cyclopamine heart (b). The cyclopamine hearts have more ground substance based on blue staining intensity around the aorta and pulmonary vessels than controls.

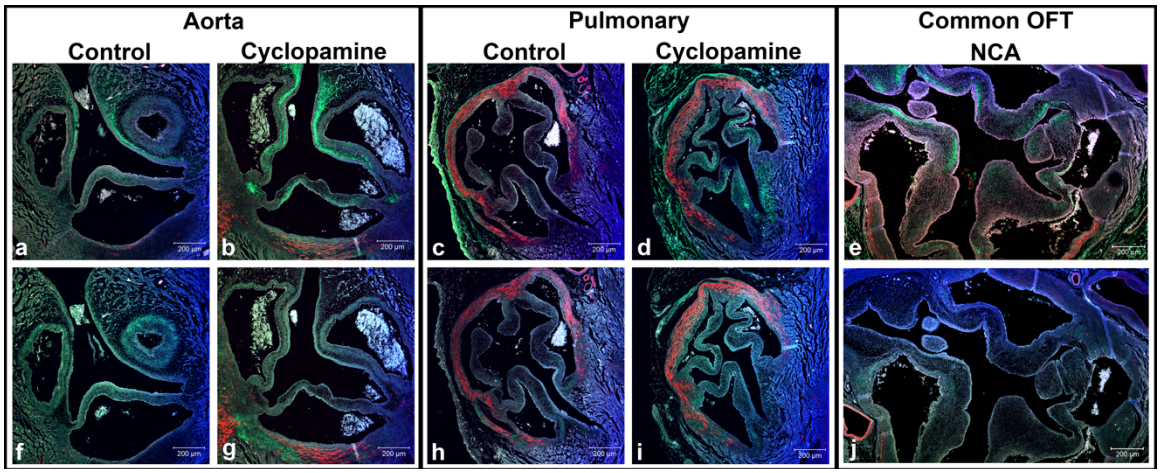

Figure A.3 shows confocal images of the aorta and pulmonary vessels of control and cyclopamine hearts as well as the common OFT in NCA hearts. Both rows of images show confocal staining of blue for cell nuclei (Dapi) and red for alpha smooth muscle actin (αSMA). The green staining on the top row is collagen type I, and the green staining on the bottom row is tenascin. The control aortas have a much more uniform shape with smaller sinuses (a, f) than the cyclopamine counterparts with less collagen type I and αSMA based on respective relative green and red staining intensity (b). The valve leaflets in the control pulmonary vessels also have more collagen type I (c) and tenascin staining (h) than the valve leaflets in the cyclopamine hearts (d, i). The common OFTs in the NCA hearts (e, j) illustrate more collagen type I and αSMA in the valve leaflets than both the control aorta and pulmonary vessels (a, c).

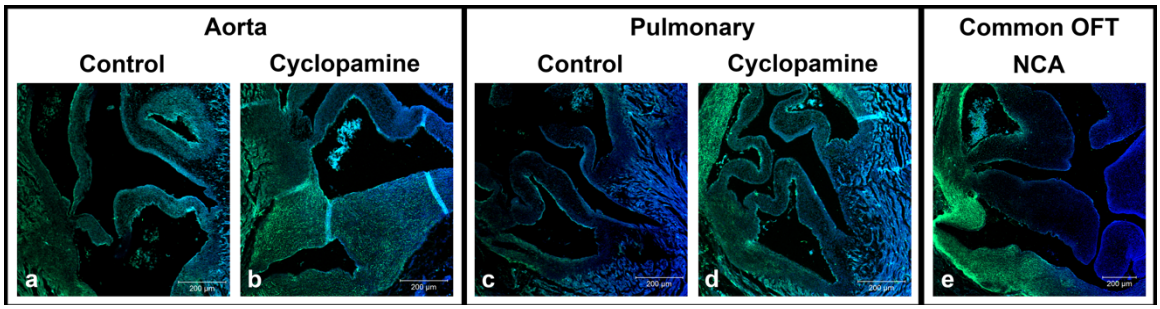

Figure A.4 shows confocal images of the aorta and pulmonary vessels of control and cyclopamine hearts as well as the common OFT in an NCA heart. The blue staining in these images is Dapi, which stains cell nuclei, and the green staining is elastin. The control aorta (a) has more even elastin staining than the cyclopamine aorta (b) as shown by relative staining intensity. The control pulmonary valve leaflets (c) are generally less cellularized and have less elastin staining intensity than the pulmonary leaflets of the cyclopamine heart (d). The NCA heart (e) demonstrates more prominent elastin around the common OFT than the vessels in the control and cyclopamine hearts (a-d) and has leaflets that are the least cellularized overall as shown by relative blue staining intensity.

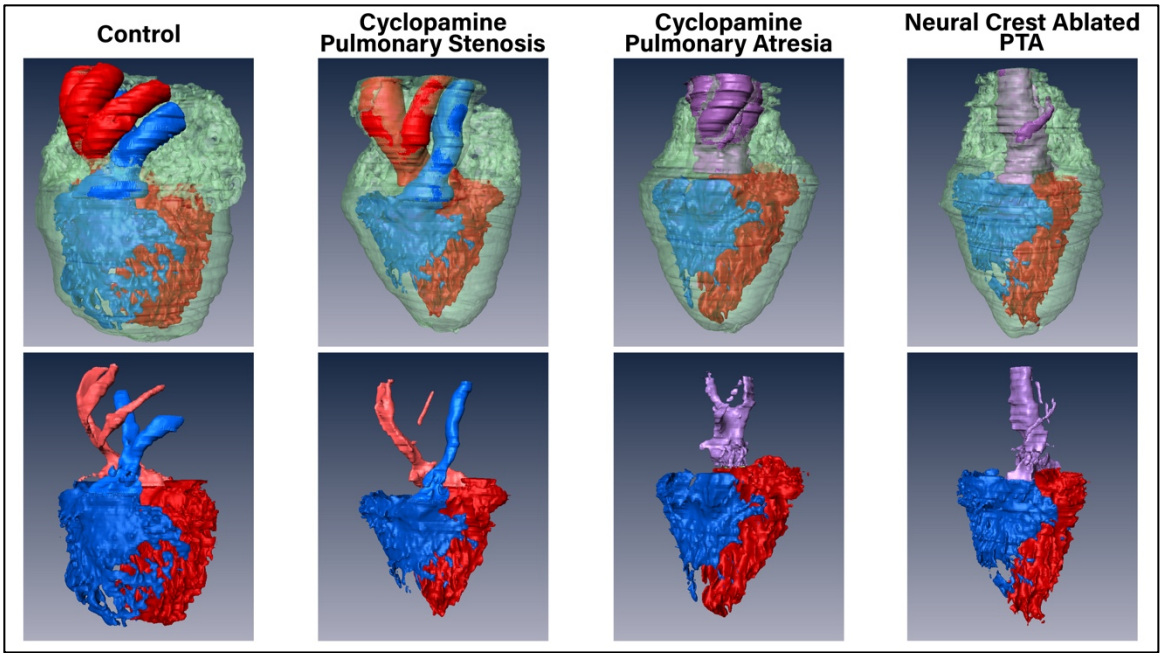

Figure A.5 Amira 3D Reconstructions of HH42 Hearts (top row) and flow space (bottom row). Control, cyclopamine-treated, and neural crest ablated hearts exhibit cardiac malformations including pulmonary stenosis, pulmonary atresia, and PTA.

APPENDIX B

PERMISSION TO REPRINT

B.1 REPRINT PERMISSION FOR CHAPTERS 1-4

CAMBRIDGE UNIVERSITY PRESS LICENSE TERMS AND CONDITIONS

Apr 18, 2019

This Agreement between Rebecca Jones ("You") and Cambridge University Press ("Cambridge University Press") consists of your license details and the terms and conditions provided by Cambridge University Press and Copyright Clearance Center.

License Number	4556130937993
License date	Mar 25, 2019
Licensed Content Publisher	Cambridge University Press
Licensed Content Publication	Microscopy and Microanalysis
Licensed Content Title	Design and Fabrication of a Three-Dimensional In Vitro System for Modeling Vascular Stenosis
Licensed Content Author	Rebecca S. Jones, Pin H. Chang, Tzlil Perahia, Katrina A. Harmon, Lorain Junor, Michael J. Yost, Daping Fan, John F. Eberth, Richard L. Goodwin
Licensed Content Date	Jul 17, 2017
Licensed Content Volume	23
Licensed Content Issue	4
Start page	859
End page	871
Type of Use	Dissertation/Thesis
Requestor type	Author
Portion	Full article
Author of this Cambridge University Press article	Yes
Author / editor of the new work	Yes
Order reference number	
Territory for reuse	North America Only
Title of your thesis / dissertation	Three-Dimensional Collagen Tubes for In Vitro Modeling
Expected completion date	May 2019
Estimated size(pages)	75

Requestor Location	Rebecca Jones 900 B West Faris Rd GREENVILLE, SC 29605 United States Attn: Rebecca Jones
Publisher Tax ID	GB823847609
Total	0.00 USD
Terms and Conditions	

TERMS & CONDITIONS

Cambridge University Press grants the Licensee permission on a non-exclusive non-transferable basis to reproduce, make available or otherwise use the Licensed content 'Content' in the named territory 'Territory' for the purpose listed 'the Use' on Page 1 of this Agreement subject to the following terms and conditions.

1. The License is limited to the permission granted and the Content detailed herein and does not extend to any other permission or content.
2. Cambridge gives no warranty or indemnity in respect of any third-party copyright material included in the Content, for which the Licensee should seek separate permission clearance.
3. The integrity of the Content must be ensured.
4. The License does extend to any edition published specifically for the use of handicapped or reading-impaired individuals.
5. The Licensee shall provide a prominent acknowledgement in the following format:
   author/s, title of article, name of journal, volume number, issue number, page references, , reproduced with permission.

Other terms and conditions:
v1.0

Questions? customercare@copyright.com or +1-855-239-3415 (toll free in the US) or +1-978-646-2777.

B.2 REPRINT PERMISSION FOR APPENDIX A

CAMBRIDGE UNIVERSITY PRESS LICENSE
TERMS AND CONDITIONS

Apr 18, 2019

This Agreement between Rebecca Jones ("You") and Cambridge University Press ("Cambridge University Press") consists of your license details and the terms and conditions provided by Cambridge University Press and Copyright Clearance Center.

License Number	4556141292179
License date	Mar 25, 2019
Licensed Content Publisher	Cambridge University Press
Licensed Content Publication	Microscopy and Microanalysis

Licensed Content Title	Conotruncal Heart Defects: Altered Tissue Morphology and Hemodynamics
Licensed Content Author	Rebecca S Jones, Lorain Junor, Mary R Hutson, Margaret L Kirby, Richard L Goodwin
Licensed Content Date	Aug 4, 2017
Licensed Content Volume	23
Licensed Content Issue	S1
Start page	1174
End page	1175
Type of Use	Dissertation/Thesis
Requestor type	Author
Portion	Full article
Author of this Cambridge University Press article	Yes
Author / editor of the new work	Yes
Order reference number	
Territory for reuse	North America Only
Title of your thesis / dissertation	Three-Dimensional Collagen Tubes for In Vitro Modeling
Expected completion date	May 2019
Estimated size(pages)	75
Requestor Location	Rebecca Jones 900 B West Faris Rd GREENVILLE, SC 29605 United States Attn: Rebecca Jones
Publisher Tax ID	GB823847609
Total	0.00 USD
Terms and Conditions	

TERMS & CONDITIONS

Cambridge University Press grants the Licensee permission on a non-exclusive non-transferable basis to reproduce, make available or otherwise use the Licensed content 'Content' in the named territory 'Territory' for the purpose listed 'the Use' on Page 1 of this Agreement subject to the following terms and conditions.

1. The License is limited to the permission granted and the Content detailed herein and does not extend to any other permission or content.
2. Cambridge gives no warranty or indemnity in respect of any third-party copyright material included in the Content, for which the Licensee should seek separate permission clearance.
3. The integrity of the Content must be ensured.
4. The License does extend to any edition published specifically for the use of handicapped or reading-impaired individuals.
5. The Licensee shall provide a prominent acknowledgement in the following format:
   author/s, title of article, name of journal, volume number, issue number, page references, , reproduced with permission.

Other terms and conditions:
v1.0

Questions? customercare@copyright.com or +1-855-239-3415 (toll free in the US) or +1-978-646-2777.